

IMPROVED METHODS FOR EMPIRICAL BAYES MULTIVARIATE MULTIPLE TESTING AND EFFECT SIZE ESTIMATION

BY YUNQI YANG¹, PETER CARBONETTO²
DAVID GERARD³ AND MATTHEW STEPHENS^{2,4,a}

¹*Committee on Genetics, Genomics and System Biology, University of Chicago*

²*Department of Human Genetics, University of Chicago*

³*Department of Mathematics and Statistics, American University*

⁴*Department of Statistics, University of Chicago, mstephens@uchicago.edu*

Estimating the sharing of genetic effects across different conditions is important to many statistical analyses of genomic data. The patterns of sharing arising from these data are often highly heterogeneous. To flexibly model these heterogeneous sharing patterns, [Urbut et al. \(2019\)](#) proposed the multivariate adaptive shrinkage (MASH) method to jointly analyze genetic effects across multiple conditions. However, multivariate analyses using MASH (as well as other multivariate analyses) require good estimates of the sharing patterns, and estimating these patterns efficiently and accurately remains challenging. Here we describe new empirical Bayes methods that provide improvements in speed and accuracy over existing methods. The two key ideas are: (1) adaptive regularization to improve accuracy in settings with many conditions; (2) improving the speed of the model fitting algorithms by exploiting analytical results on covariance estimation. In simulations, we show that the new methods provide better model fits, better out-of-sample performance, and improved power and accuracy in detecting the true underlying signals. In an analysis of eQTLs in 49 human tissues, our new analysis pipeline achieves better model fits and better out-of-sample performance than the existing MASH analysis pipeline. We have implemented the new methods, which we call “Ultimate Deconvolution”, in an R package, `udr`, available on GitHub.

1. Introduction. The problem of testing and estimating effect sizes for many units in multiple conditions (or on multiple outcomes) arises frequently in genomics applications. Examples include assessing the effects of many expression quantitative trait loci (eQTLs) in multiple tissues ([GTEx Consortium et al., 2015](#)) and assessing the effects of many genetic variants on multiple traits ([Zhou and Stephens, 2014](#); [Pickrell et al., 2016](#); [Turchin and Stephens, 2019](#); [Udler et al., 2018](#); [Zou et al., 2024](#)). The simplest approach to assessing effects in multiple conditions is to analyze each condition separately. However, this fails to exploit sharing or similarity of effects among conditions. For example, a genetic variant that increases expression of a particular gene in the heart may similarly increase expression in other tissues, particularly in tissues that are related to heart. Such sharing of effects could be exploited to improve power and estimation accuracy by borrowing information across conditions. This is, in essence, the motivation for meta-analysis methods ([Willer, Li and Abecasis, 2010](#); [Han and Eskin, 2011](#); [Wen and Stephens, 2014](#)), and more generally it motivates consideration of multivariate approaches to multiple testing and effect size estimation ([Urbut et al., 2019](#)).

Keywords and phrases: multivariate analysis, empirical Bayes, normal means, multiple testing, adaptive shrinkage, expectation maximization.

While borrowing information across conditions may be a natural idea, getting it to work well in practice requires confronting some thorny issues. One challenge is that the extent to which effects are shared among conditions will vary among data sets; for example, data sets involving very similar conditions may have very high levels of sharing, whereas data sets involving very different conditions may exhibit little to no sharing. Furthermore, some data sets may include some conditions that are very similar and others that are very dissimilar, and these differences may be difficult to specify in advance. Assessing the sharing and similarity of effects among conditions may also be an important goal in itself.

Empirical Bayes (EB) approaches (e.g., [Flutre et al. 2013](#); [Urbut et al. 2019](#)) provide an attractive way to confront these challenges. EB methods estimate a prior distribution that captures the sharing or similarity of effects among the conditions, then, using Bayes theorem, they combine the prior with the observed data to improve the effect estimates. The methods proposed in [Urbut et al. \(2019\)](#) and implemented in the R package `mashr` assume a mixture of multivariate normal distributions for the prior, which has the twin advantages of being both both flexible and computationally convenient. Indeed, `mashr` has been used to analyze very large data sets involving many conditions ([Zou et al., 2024](#); [Lin et al., 2024](#); [Urbut et al., 2021](#); [Barbeira et al., 2020](#); [Araujo et al., 2023](#); [Li et al., 2022](#); [Soliai et al., 2021](#); [Natri et al., 2024](#); [Bonder et al., 2021](#)).

Despite this, these methods still have considerable limitations; in particular, fitting a mixture of multivariate normals prior with unknown covariance matrices raises statistical and computational challenges. [Urbut et al. \(2019\)](#) used a two-stage procedure to deal with (or sidestep) these challenges: in the first stage, the covariance matrices in the prior were estimated by maximum-likelihood on a subset of the data (using the “Extreme Deconvolution” algorithm of [Bovy, Hogg and Roweis 2011](#)); next, given the covariances estimated in the first stage, the second stage estimated the mixture proportions in the prior by maximizing the likelihood from all the data (using the fast optimization algorithms of [Kim et al. 2020](#)). The second stage is a convex optimization problem, and can be solved efficiently and reliably for very large data sets. The first stage, however, presents several challenges, including that the Extreme Deconvolution (ED) algorithm can be slow to converge, the results of running ED are often sensitive to initialization, and the estimated covariance matrices can be quite unstable, particularly when the number of conditions, R , is large relative to sample size, n . These challenges motivated this work, which is a closer examination of these challenges from both a statistical perspective and a computational one. One of the contributions of this study is a new algorithm, which we call “truncated eigenvalue decomposition” (TED). TED often converges much faster than ED. (Noting that ED applies to some settings where TED does not.) We also explore the use of simple regularization schemes that can improve accuracy compared with maximum-likelihood estimation, particularly when the sample size n is small and the number of conditions R is large (that is, the ratio R/n is large). And we highlight some problems that arise from using low-rank covariance matrices, which was a strategy previously suggested in [Urbut et al. \(2019\)](#) to reduce the number of estimated parameters. We provide an R package, `udr` (“Ultimate Deconvolution in R”), available at <https://github.com/stephenslab/udr>, which implements all these methods described here within a convenient, user-friendly interface, and that interacts well with our previous R package, `mashr` ([Urbut et al., 2019](#)). The version of the R package used to perform the analyses in this manuscript is also available for download as a supplementary file ([Yang, Carbonetto and Stephens, 2024a](#)).

The paper is structured as follows. Section 2 summarizes notation used in the mathematical expressions throughout the paper. Section 3 formally introduces the models, priors and regularization schemes considered, and Section 4 describes the model-fitting algorithms and procedures. Section 5 evaluates the performance of the different methods and algorithms on data sets simulated under a variety of scenarios. Section 6 applies the improved methods to an analysis of a large, multi-tissue eQTL data set from the GTEx Project. Finally, Section 7 discusses the promise and limitations of our methods, and future directions.

2. Notation used in the mathematical expressions. For the mathematical expressions below, we use bold, capital letters (\mathbf{A}) to denote matrices; bold, lowercase letters (\mathbf{a}) to denote column vectors; and plain, lowercase letters (a) to denote scalars. For a matrix \mathbf{A} , $\|\mathbf{A}\|_*$ denotes its nuclear norm, \mathbf{A}^T denotes its transpose, \mathbf{A}^{-1} denotes its inverse, \mathbf{A}^{-T} denotes the inverse of \mathbf{A}^T , $\text{tr}(\mathbf{A})$ denotes the trace, and $|\mathbf{A}|$ denotes the matrix determinant. We use $\mathbf{0}$ and $\mathbf{1}$ to denote the vectors whose elements are all zeros and all ones respectively; \mathbf{e}_r for the standard basis vector $\mathbf{e}_r = (0, \dots, 0, 1, 0, \dots, 0)$ with the 1 appearing in the r th position; \mathbf{I}_R is the $R \times R$ identity matrix; and $\text{diag}(\mathbf{a})$ denotes the diagonal matrix in which the diagonal entries are given by the entries of vector \mathbf{a} . We use \mathbb{R} for the set of real numbers, \mathbb{R}^R for the set of real-valued vectors of length R , and $\mathbb{R}^{n \times m}$ for the set of real-valued $n \times m$ matrices. We use $N(\mu, \sigma^2)$ to denote the normal distribution on \mathbb{R} with mean μ and variance σ^2 , and $N(\cdot; \mu, \sigma^2)$ denotes its density. And we use $N_R(\boldsymbol{\mu}, \boldsymbol{\Sigma})$ for the multivariate normal distribution on \mathbb{R}^R with mean $\boldsymbol{\mu} \in \mathbb{R}^R$ and $R \times R$ covariance matrix $\boldsymbol{\Sigma}$, and $N_R(\cdot; \boldsymbol{\mu}, \boldsymbol{\Sigma})$ denotes its density. We use $P_R^+ \subseteq \mathbb{R}^{R \times R}$ to denote the set of real-valued $R \times R$ (symmetric) positive semi-definite matrices. $\mathcal{S}_R \subseteq \mathbb{R}^R$ denotes the R -dimensional simplex.

3. The empirical Bayes multivariate normal means model. In this section, we define the “empirical Bayes multivariate normal means” (EBMNM) model. We describe several variations of this model that involve constraints or penalties on the model parameters.

The EBMNM model assumes that we observe vectors $\mathbf{x}_j \in \mathbb{R}^R$, that are independent, noisy, normally-distributed measurements of underlying true values $\boldsymbol{\theta}_j \in \mathbb{R}^R$:

$$(1) \quad \mathbf{x}_j | \boldsymbol{\theta}_j \sim N_R(\boldsymbol{\theta}_j, \mathbf{V}_j), \quad j = 1, \dots, n,$$

in which the covariances $\mathbf{V}_j \in P_R^+$ are assumed to be known and invertible. Our ultimate goal is to perform inference for the unknown means $\boldsymbol{\theta}_j$ from the observed data \mathbf{x}_j . This model is a natural generalization of the well-studied (univariate) normal means model (Robbins, 1951; Efron and Morris, 1972; Stephens, 2017; Bhadra et al., 2019; Johnstone, 2019; Sun, 2020), and so we call it the “multivariate normal means model”. An important special case is when the measurement error distribution is the same for all observations; i.e., $\mathbf{V}_j = \mathbf{V}$, $j = 1, \dots, n$. We refer to this as the “homoskedastic” case. Some of our computational methods are designed specifically for the homoskedastic case, which is easier to solve than the “heteroskedastic” case.

The EBMNM model (1) further assumes that the unknown means are independent and identically distributed draws from some distribution, which we refer to as the “prior distribution”. While other choices are possible, here we assume the prior distribution is a mixture of zero-mean multivariate normals:

$$(2) \quad p(\boldsymbol{\theta}_j | \boldsymbol{\pi}, \mathcal{U}) = \sum_{k=1}^K \pi_k N_R(\boldsymbol{\theta}_j; \mathbf{0}, \mathbf{U}_k),$$

where $\boldsymbol{\pi} \in \mathcal{S}_K$ is the set of mixture proportions, $\mathbf{U}_k \in P_R^+$ are covariance matrices, and $\mathcal{U} := \{\mathbf{U}_1, \dots, \mathbf{U}_K\}$ denotes the full collection of covariance matrices.

Combining (1) and (2) yields the marginal distribution

$$(3) \quad p(\mathbf{x}_j | \boldsymbol{\pi}, \mathcal{U}) = \sum_{k=1}^K \pi_k N_R(\mathbf{x}_j; \mathbf{0}, \mathbf{U}_k + \mathbf{V}_j),$$

and the marginal log-likelihood,

$$\ell(\boldsymbol{\pi}, \mathcal{U}) := \sum_{j=1}^n \log p(\mathbf{x}_j | \boldsymbol{\pi}, \mathcal{U})$$

$$(4) \quad = \sum_{j=1}^n \log \sum_{k=1}^K \pi_k N_R(\mathbf{x}_j; \mathbf{0}, \mathbf{U}_k + \mathbf{V}_j)$$

The EB approach to fitting the model (1–2) proceeds in two stages:

1. Estimate the prior parameters $\boldsymbol{\pi}, \mathcal{U}$ by maximizing a penalized log-likelihood,

$$(5) \quad (\hat{\boldsymbol{\pi}}, \hat{\mathcal{U}}) := \underset{\boldsymbol{\pi} \in \mathcal{S}_K, \mathbf{U}_k \in P_R^{+,k}}{\operatorname{argmax}} \quad \ell(\boldsymbol{\pi}, \mathcal{U}) - \sum_{k=1}^K \tilde{\rho}(\mathbf{U}_k),$$

where $\tilde{\rho}$ denotes a penalty function introduced to regularize \mathbf{U}_k , and $P_R^{+,k} \subseteq P_R^+$ allows for constraints on \mathbf{U}_k (which may be different for each component of the mixture). The exact penalties and constraints considered are described below. When $P_R^{+,k} = P_R^+$ and $\tilde{\rho}(\mathbf{U}_k) = 0$ for all \mathbf{U}_k , solving (5) corresponds to maximum-likelihood estimation of $\boldsymbol{\pi}, \mathcal{U}$.

2. Compute the posterior distribution for each $\boldsymbol{\theta}_j$ given $\boldsymbol{\pi}, \mathcal{U}$ estimated in the first stage:

$$(6) \quad \begin{aligned} p_{\text{post}}(\boldsymbol{\theta}_j) &:= p(\boldsymbol{\theta}_j \mid \mathbf{x}_j, \hat{\boldsymbol{\pi}}, \hat{\mathcal{U}}) \\ &\propto p(\mathbf{x}_j \mid \boldsymbol{\theta}_j) p(\boldsymbol{\theta}_j \mid \hat{\boldsymbol{\pi}}, \hat{\mathcal{U}}). \end{aligned}$$

The posterior distributions (6) have an analytic form, and are mixtures of multivariate normal distributions (see for example [Urbut et al. 2019](#); [Bovy, Hogg and Roweis 2011](#)) and Section 1.1 of the Supplementary Materials; [Yang, Carbonetto and Stephens 2024b](#)). Since these posterior distributions have a closed form, it is relatively straightforward to compute posterior summaries such as the posterior mean and posterior standard deviation, and measures for significance testing such as the *local false sign rate* (*lfsr*) ([Stephens, 2017](#)). Therefore, we focus on methods for accomplishing the first step, solving (5).

3.1. A reformulation to ensure scale invariance. Intuitively, one might hope that changing the units of measurement of all the observed \mathbf{x}_j would simply result in corresponding changes to the units of the estimated $\boldsymbol{\theta}_j$. This idea can be formalized as requiring that solutions of the EBMNM model should obey a “scale invariance” property. This consideration motivates us to reformulate (5). Let $\hat{\boldsymbol{\theta}}_j(\mathbf{x}_1, \dots, \mathbf{x}_n, \mathbf{V}_1, \dots, \mathbf{V}_n)$ denote the posterior mean for $\boldsymbol{\theta}_j$ computed by solving the EBMNM problem with data $\mathbf{x}_1, \dots, \mathbf{x}_n, \mathbf{V}_1, \dots, \mathbf{V}_n$. We say that the solution is “scale invariant” if, for any $s > 0$, the following holds:

$$(7) \quad \hat{\boldsymbol{\theta}}_j(s\mathbf{x}_1, \dots, s\mathbf{x}_n, s^2\mathbf{V}_1, \dots, s^2\mathbf{V}_n) = s\hat{\boldsymbol{\theta}}_j(\mathbf{x}_1, \dots, \mathbf{x}_n, \mathbf{V}_1, \dots, \mathbf{V}_n).$$

That is, multiplying all the observed data points by s (which multiplies the corresponding error variance by s^2) has the effect of multiplying the estimated means by s . (Note: we state scale invariance in terms of the posterior means only for simplicity; the concept is easily generalized to require that the whole posterior distribution for $\boldsymbol{\theta}_j$ scales similarly.)

Without the penalty $\tilde{\rho}$ in (5), it is easy to show that the scale invariance property (7) holds provided that the constraints satisfy $\mathbf{U}_k \in P_R^{+,k} \implies s_k \mathbf{U}_k \in P_R^{+,k}, \forall s_k > 0$. With penalty, scale invariance holds provided that $\tilde{\rho}(\mathbf{U}) = \tilde{\rho}(s\mathbf{U}), \forall s, \mathbf{U}$; that is, provided that the penalty function depends only on the “shape” of \mathbf{U} and not on its “scale”. To ensure scale invariance, we therefore consider penalties of the form

$$(8) \quad \tilde{\rho}(\mathbf{U}) = \min_{s>0} \rho(\mathbf{U}/s),$$

where ρ is a penalty that may depend on both the shape and scale of \mathbf{U} . To give some intuition, suppose that ρ encourages all the eigenvalues of \mathbf{U} to be close to 1. Then $\tilde{\rho}$ will

encourage the eigenvalues to be close to each other, without requiring that they specifically be close to 1. Therefore, plugging (8) into (5), we have

$$(9) \quad (\hat{\boldsymbol{\pi}}, \hat{\mathcal{U}}) := \underset{\boldsymbol{\pi} \in \mathcal{S}_K, \mathbf{U}_k \in P_R^{+,k}, \mathbf{s} > \mathbf{0}}{\operatorname{argmax}} \quad \ell(\boldsymbol{\pi}, \mathcal{U}) - \sum_{k=1}^K \rho(\mathbf{U}_k / s_k),$$

where $\mathbf{s} := (s_1, \dots, s_K)$. We use (9) for the remainder of the paper.

3.2. Constraints and penalties. Estimating covariance matrices in high-dimensional settings (*i.e.*, large R) is known to be a challenging problem (e.g., [Johnstone and Paul 2018](#); [Fan, Liao and Liu 2016](#); [Ledoit and Wolf 2022](#)). Even in the simpler setting of independent and identically distributed observations from a single multivariate normal distribution, the maximum-likelihood estimate of the covariance matrix can be unstable, and so various covariance regularization approaches have been proposed to address this issue ([Ledoit and Wolf, 2004](#); [Friedman, Hastie and Tibshirani, 2008](#); [Cai and Liu, 2011](#); [Won et al., 2013](#); [Chi and Lange, 2014](#)). Interestingly, in the context of using EBMNM for significance testing, adding penalties have additional benefits (see the numerical experiments below).

We consider two different penalties that have been previously used for covariance regularization:

1. The ‘‘inverse Wishart’’ (IW) penalty

$$(10) \quad \rho_{\lambda}^{\text{IW}}(\mathbf{U}) := \frac{\lambda}{2} \{\log |\mathbf{U}| + \operatorname{tr}(\mathbf{U}^{-1})\}$$

$$(11) \quad = \frac{\lambda}{2} \sum_{r=1}^R (\log e_r + 1/e_r).$$

2. The ‘‘nuclear norm’’ (NN) penalty:

$$(12) \quad \rho_{\lambda}^{\text{NN}}(\mathbf{U}) := \frac{\lambda}{2} \{0.5 \|\mathbf{U}\|_* + 0.5 \|\mathbf{U}^{-1}\|_*\}$$

$$(13) \quad = \frac{\lambda}{2} \sum_{r=1}^R (0.5 e_r + 0.5 / e_r).$$

Here, e_1, \dots, e_R denote the eigenvalues of \mathbf{U} , and $\lambda > 0$ controls the strength of the penalty. We chose $\lambda = R$ in our simulations, but one could also use cross-validation to select λ .

The IW penalty on \mathbf{U}_k corresponds to *maximum a posteriori* (MAP) estimation of \mathbf{U}_k under an inverse-Wishart prior, with prior mode \mathbf{I}_R and $\lambda - R - 1$ degrees of freedom ([Fraleigh and Raftery, 2007](#)). This penalty was also mentioned (but not used or evaluated) in [Bovy, Hogg and Roweis \(2011\)](#).

The nuclear norm penalty was studied as an alternative to the IW penalty for estimation of covariance matrices in [Chi and Lange \(2014\)](#). To our knowledge, this penalty has not been studied in the EBMNM setting. The nuclear norm penalty in [Chi and Lange \(2014\)](#) includes a hyperparameter $\alpha \in (0, 1)$ that controls the balance between $\|\mathbf{U}\|_*$ and $\|\mathbf{U}^{-1}\|_*$, but our approach to ensuring scale-invariance has the consequence that changing α is equivalent to changing λ (see the Supplementary Materials; [Yang, Carbonetto and Stephens 2024b](#)), so we set $\alpha = 0.5$.

As can be seen from (11) and (13), both penalties depend only on the eigenvalues of \mathbf{U} , and decompose into additive functions of the R eigenvalues. Both penalties are minimized when $\mathbf{U} = \mathbf{I}_R$, and more generally encourage \mathbf{U} to be well-conditioned by making it closer to the identity matrix (by pushing the eigenvalues closer to 1).

As an alternative to penalized estimation of \mathbf{U} , we also consider estimating \mathbf{U} under different constraints:

TABLE 1

Summary of the EBMNM algorithms and the situations in which they apply. In this table we consider 4 variations of EBMNM: no constraint on \mathbf{U} or a rank-1 constraint; and homoskedastic (hom.) errors (all \mathbf{V}_j are the same) or heteroskedastic (het.) errors (one or more \mathbf{V}_j differ). Abbreviations used in this table are: ED = Extreme Deconvolution), FA = factor analysis, TED = truncated eigenvalue decomposition. A checkmark (\checkmark) indicates that the algorithm (ED, FA, TED) can be applied to the particular variation. Note that fitting \mathbf{U} with a scaling constraint involves only a 1-d optimization and is treated separately.

algorithm	constraints on \mathbf{U}			
	none		rank-1	
	hom.	het.	hom.	het.
ED	\checkmark	\checkmark		
FA	\checkmark		\checkmark	\checkmark
TED	\checkmark		\checkmark	

1. A scaling constraint, $\mathbf{U}_k = c_k \mathbf{U}_{0k}$, for some chosen $\mathbf{U}_{0k} \in P_R^+$.
2. A rank-1 constraint, $\mathbf{U}_k = \mathbf{u}_k \mathbf{u}_k^T$, for some $\mathbf{u}_k \in \mathbb{R}^R$.

The scaling constraint could be useful for situations in which the θ_j may obey an expected sharing structure, or for sharing structures that are easier to interpret. For example, $\mathbf{U}_{0k} = \mathbf{I}_R$ captures the situation in which all the effects $\theta_{j1}, \dots, \theta_{jR}$ are independent, and $\mathbf{U}_{0k} = \mathbf{1}\mathbf{1}^T$ captures the situation in which all the effects $\theta_{j1}, \dots, \theta_{jR}$ are equal. Such covariances are referred to as ‘‘canonical’’ covariance matrices in [Urbut et al. \(2019\)](#).

The rank-1 constraint also leads to potentially more interpretable covariance matrices, and can be thought of as a form of regularization because low-rank matrices have fewer parameters to be estimated. It may also allow for faster computations. [Urbut et al. \(2019\)](#) in fact make extensive use of the rank-1 constraint. However, our results will show that this constraint can cause problems for significance testing and so may be better avoided in practice.

4. Fitting the EBMNM model. We now describe three algorithms we have implemented for fitting variations of the EBMNM model described above: the ED algorithm from [Bovy, Hogg and Roweis 2011](#); an algorithm based on methods commonly used in factor analysis (FA); and another based on the truncated eigenvalue decomposition (TED). Each of these algorithms applies to a subset of EBMNM models (Table 1). In some situations, only one algorithm can be applied; for example, only ED can handle heteroskedastic variances with no constraints on \mathbf{U} . However, in other settings all three algorithms can be applied (e.g., homoskedastic errors, no constraints on \mathbf{U}). Below, we empirically assess the relative merits of the different algorithms in simulations that model these different settings. See also Supplementary Tables 1 and 2 ([Yang, Carbonetto and Stephens, 2024b](#)) for a comparison of the algorithms’ computational properties in the different settings.

4.1. *Algorithms for the single-component EBMNM model with no penalty.* While these algorithms are implemented for the mixture prior (2) with the penalties described above, the algorithms are much easier to describe in the special case of one mixture component ($K = 1$), and without penalty. So initially we focus on this simpler case, and later we extend to the general form with penalties and $K \geq 1$.

With $K = 1$ and no penalty, the prior is $\theta_j \sim N(\mathbf{0}, \mathbf{U})$, the model is

$$(14) \quad \mathbf{x}_j | \mathbf{U} \sim N_R(\mathbf{0}, \mathbf{U} + \mathbf{V}_j), \quad j = 1, \dots, n.$$

and the goal is to compute the maximum-likelihood estimate of \mathbf{U} :

$$(15) \quad \hat{\mathbf{U}} := \operatorname{argmax}_{\mathbf{U} \in P_R^+} \sum_{j=1}^n \log N_R(\mathbf{x}_j; \mathbf{0}, \mathbf{U} + \mathbf{V}_j)$$

The three algorithms for solving (15) are as follows.

Truncated Eigenvalue Decomposition (TED). This algorithm, which to the best of our knowledge is new in this context, exploits the fact that, in the special case where $\mathbf{V}_j = \mathbf{I}_R$, $j = 1, \dots, n$, the maximum-likelihood estimate (15) can be computed exactly. At first glance, one might try to solve for $\hat{\mathbf{U}}$ by setting $\hat{\mathbf{U}} + \mathbf{I}_R$ to the sample covariance matrix, $\mathbf{S} := \sum_{j=1}^n \mathbf{x}_j \mathbf{x}_j^T / n$, then recovering $\hat{\mathbf{U}}$ as $\hat{\mathbf{U}} = \mathbf{S} - \mathbf{I}_R$. However, $\mathbf{S} - \mathbf{I}_R$ is not necessarily a positive semi-definite matrix; that is, it may have one or more eigenvalues that are negative. One could deal with this problem by setting the negative eigenvalues to zero, and indeed this approach is correct; that is, letting $(\mathbf{S})_+$ be the matrix obtained from \mathbf{S} by truncating its negative eigenvalues to 0, $\hat{\mathbf{U}} = (\mathbf{S} - \mathbf{I}_R)_+$ is the maximum-likelihood estimate of \mathbf{U} (Tipping and Bishop, 1999). This idea can also be used to solve the more general case, $\mathbf{V}_j = \mathbf{V}$, essentially by transforming the data to $\mathbf{R}^{-1} \mathbf{x}_j$ where $\mathbf{V} = \mathbf{R} \mathbf{R}^T$, estimating $\mathbf{R}^{-1} \mathbf{U} \mathbf{R}^{-T}$ from this transformed data, then reversing this transformation, see Yang, Carbonetto and Stephens 2024b.

Extreme Deconvolution (ED). This is an EM algorithm (Dempster, Laird and Rubin, 1977), an iterative approach to solving (15); the name comes from Bovy, Hogg and Roweis (2011). ED uses the natural “data augmentation” representation of (14):

$$(16) \quad \begin{aligned} \boldsymbol{\theta}_j &\sim N_R(\mathbf{0}, \mathbf{U}) \\ \mathbf{x}_j \mid \boldsymbol{\theta}_j &\sim N_R(\boldsymbol{\theta}_j, \mathbf{V}_j). \end{aligned}$$

Following the usual EM derivation, the updates can be derived as

$$(17) \quad \mathbf{U}^{\text{new}} = \frac{1}{n} \sum_{j=1}^n \mathbf{B}_j + \mathbf{b}_j \mathbf{b}_j^T,$$

where \mathbf{b}_j and \mathbf{B}_j are, respectively, the posterior mean and covariance of $\boldsymbol{\theta}_j$ given \mathbf{U} :

$$(18) \quad \mathbf{b}_j := \mathbf{U}(\mathbf{U} + \mathbf{V}_j)^{-1} \mathbf{x}_j$$

$$(19) \quad \mathbf{B}_j := \mathbf{U} - \mathbf{U}(\mathbf{U} + \mathbf{V}_j)^{-1} \mathbf{U}.$$

The update (17) is guaranteed to increase (or not decrease) the objective function in (15), and repeated application of (17–19) will converge to a stationary point of the objective.

Factor analysis (FA). This is also an EM algorithm, but based on a different data augmentation than ED; the name comes from its close connection to EM algorithms for factor analysis models (Ghahramani and Hinton, 1996; Rubin and Thayer, 1982; Zhao, Philip and Jiang, 2008; Liu and Rubin, 1998; McLachlan and Peel, 2000). In its simplest form, the FA approach imposes a rank-1 constraint on \mathbf{U} , $\mathbf{U} = \mathbf{u} \mathbf{u}^T$, where $\mathbf{u} \in \mathbb{R}^R$ is to be estimated. The model (14) then admits the following data augmentation representation:

$$(20) \quad \begin{aligned} a_j &\sim N(0, 1) \\ \mathbf{x}_j \mid \mathbf{u}, \mathbf{V}_j, a_j &\sim N(a_j \mathbf{u}, \mathbf{V}_j). \end{aligned}$$

The usual EM derivation gives the update

$$(21) \quad \mathbf{u}^{\text{new}} = \left(\sum_{j=1}^n (\mu_j^2 + \sigma_j^2) \mathbf{V}_j^{-1} \right)^{-1} \left(\sum_{j=1}^n \mu_j \mathbf{V}_j^{-1} \mathbf{x}_j \right),$$

in which μ_j and σ_j^2 denote, respectively, the posterior mean and posterior covariance of a_j given \mathbf{u} ,

$$(22) \quad \mu_j := \sigma_j^2 \mathbf{u}^T \mathbf{V}_j^{-1} \mathbf{x}_j$$

$$(23) \quad \sigma_j^2 := 1 / (1 + \mathbf{u}^T \mathbf{V}_j^{-1} \mathbf{u}).$$

Input: Data vectors $\mathbf{x}_j \in \mathbb{R}^R$ and corresponding covariance matrices $\mathbf{V}_j \in P_R^+$, $j = 1, \dots, n$; K , the number of mixture components; initial estimates of the prior covariance matrices $\mathcal{U} = \{\mathbf{U}_1, \dots, \mathbf{U}_K\}$, $\mathbf{U}_k \in P_R^{+,k}$, $k = 1, \dots, K$; initial estimates of the scaling parameters $\mathbf{s} = \{s_1, \dots, s_K\} \in \mathbb{R}^K$; initial estimates of the mixture weights $\boldsymbol{\pi} \in \mathcal{S}_K$.

Output: \mathcal{U} , $\boldsymbol{\pi}$.

repeat

for $j \leftarrow 1$ **to** n **do**

for $k \leftarrow 1$ **to** K **do**

 Update w_{jk} using (24).

end

end

for $k \leftarrow 1$ **to** K **do**

$\pi_k \leftarrow \sum_{j=1}^n w_{jk} / n$

$\mathbf{U}_k \leftarrow \operatorname{argmax}_{\mathbf{U} \in P_R^{+,k}} \phi(\mathbf{U}; \mathbf{w}_k) - \rho(\mathbf{U}/s_k)$

 ▷ Note that some algorithms compute this argmax inexactly.

$s_k \leftarrow \operatorname{argmin}_{s > 0} \rho(\mathbf{U}_k/s)$

end

until convergence criterion is met;

Algorithm 1: EM for fitting the EBMNM model.

The update (21) is guaranteed to increase (or not decrease) the objective function in (15), and repeated application of (21–23) will converge to a stationary point of the objective. These updates can be extended to higher-rank covariances where the goal is to find the maximum-likelihood estimate subject of \mathbf{U} subject to \mathbf{U} having rank at most R' , where $R' \leq R$. However, when $R' > 1$, the updates are have closed-form expressions only for homoskedastic errors, $\mathbf{V}_j = \mathbf{V}$.

The three algorithms have different strengths and weaknesses, and settings to which they apply (Table 1). The TED algorithm has the advantage of directly computing the maximum-likelihood estimate, which seems preferable to an iterative approach. However, TED only applies in the case of homoskedastic errors. The ED approach is more general, applying to both heteroskedastic and homoskedastic errors, although it cannot fit rank-1 matrices. The FA approach is attractive for low-rank matrices, particularly for fitting rank-1 matrices.

Our claim that ED cannot fit rank-1 covariance matrices deserves discussion, especially since [Urbut et al. \(2019\)](#) used ED to fit such matrices. As pointed out by [Urbut et al. \(2019\)](#), if ED is initialized to a low-rank matrix with rank R' , then the updated estimates (17) are also rank (at most) R' . Thus, if ED is initialized to a rank-1 matrix, the final estimate is also rank-1. However, the ED estimates are not only low rank, but also span the same subspace as the initial estimates, a property we refer to as “subspace-preserving”. Thus, if ED is initialized to $\mathbf{U} = \mathbf{u}\mathbf{u}^T$, the updated estimates will be of the form $a\mathbf{u}\mathbf{u}^T$ for some scalar a . In other words, the ED update does not change rank-1 matrices, except by a scaling factor, and so the final estimate will simply be proportional to the initial estimate. This flaw motivated us to implement the FA method. However, as our numerical comparisons will illustrate, the rank-1 matrices turn out to have other drawbacks that lead us not to recommend their use anyhow.

4.2. Extending the algorithms to a mixture prior. All of the algorithms—TED, ED and FA—can be generalized from the $K = 1$ case to the $K \geq 1$ case using the standard EM approach to dealing with mixtures. The resulting algorithms have a simple common structure, summarized in Algorithm 1. (This algorithm also allows for an inclusion of a penalty, which is treated in the next section. See also the Supplementary Materials for a derivation of this algorithm; [Yang, Carbonetto and Stephens 2024b](#).) This EM algorithm involves iterating the following steps: (i) compute the weights, w_{jk} (sometimes called the “responsibilities”), each

which represent the conditional probability that mixture component k gave rise to observation j given the current estimates of $\boldsymbol{\pi}, \mathcal{U}$,

$$(24) \quad w_{jk} = \frac{\pi_k N_R(\mathbf{x}_j; \mathbf{0}, \mathbf{U}_k + \mathbf{V}_j)}{\sum_{k'=1}^K \pi_{k'} N_R(\mathbf{x}_j; \mathbf{0}, \mathbf{U}_{k'} + \mathbf{V}_j)};$$

(ii) update $\boldsymbol{\pi}$ by averaging the weights (this is the standard EM update for estimating mixture proportions, and is the same for all the algorithms); (iii) update the covariance matrices \mathcal{U} (this is the step where the algorithms differ); and (iv) update the scaling parameters, \mathbf{s} . (The update of the scaling parameters is the same for all algorithms, and depends on the chosen penalty. For details, see the Supplementary Materials; [Yang, Carbonetto and Stephens 2024b](#).)

With this data augmentation, the updates for the covariance matrices \mathbf{U}_k have the following form:

$$(25) \quad \mathbf{U}^{\text{new}} = \underset{\mathbf{U} \in P_R^{+,k}}{\operatorname{argmax}} \phi(\mathbf{U}; \mathbf{w}_k),$$

where

$$(26) \quad \phi(\mathbf{U}; \mathbf{w}) := \sum_{j=1}^n w_j \log N_R(\mathbf{x}_j; \mathbf{0}, \mathbf{U} + \mathbf{V}_j).$$

The function ϕ can be viewed as a *weighted* version of the log-likelihood with normal prior (14), and the updates for this weighted problem are very similar to the updates for a normal prior. For example, the TED update, which solves the weighted problem exactly in the case $\mathbf{V}_j = \mathbf{I}_R$, involves truncating the eigenvalues of $\hat{\mathbf{S}} - \mathbf{I}_R$ where $\hat{\mathbf{S}} := \sum_{j=1}^n w_j \mathbf{x}_j \mathbf{x}_j^T / (\sum_{j=1}^n w_j)$ is *the weighted sample covariance matrix*. Details of the TED, ED and FA updates for weighted log-likelihoods are given in the Supplementary Text ([Yang, Carbonetto and Stephens, 2024b](#)).

4.3. *Modifications to the algorithms to incorporate the penalties.* With a penalty, the updates (25) are instead

$$(27) \quad \mathbf{U}^{\text{new}} = \underset{\mathbf{U} \in P_R^{+,k}, s_k > 0}{\operatorname{argmax}} \phi(\mathbf{U}; \mathbf{w}_k) - \rho(\mathbf{U}/s_k).$$

We have adapted the TED approach, in the case $\mathbf{V}_j = \mathbf{I}_R$, to incorporate either the IW or NN penalty. These extensions replace the simple truncation of the eigenvalues with solving a (1-d) optimization problem for each eigenvalue e_r ; while these 1-d optimization problems do not have closed form solutions, they are easily solved using off-the-shelf numerical methods. This approach can also be applied, via the data transformation approach, to the general homoskedastic case $\mathbf{V}_j = \mathbf{V}$; however, this transformation approach implicitly changes the penalty so that it encourages \mathbf{U}_k/s_k to be close to \mathbf{V} rather than being close to \mathbf{I}_R . This change in the penalty appears to be necessary to make the TED approach work when $\mathbf{V} \neq \mathbf{I}_R$. See the Supplementary Materials ([Yang, Carbonetto and Stephens, 2024b](#)) for details.

Incorporating an IW penalty into the ED approach is also straightforward ([Bovy, Hogg and Roweis, 2011](#)) and results in a simple change to the closed-form updates (17). The NN penalty does not result in closed-form updates for ED and so we have not implemented it.

Incorporating penalties into the FA updates may be possible but we have not done so.

4.4. *Significance testing.* In EBMNM, inferences are based on the posterior distribution, $p_{\text{post}}(\boldsymbol{\theta}_j) = p(\boldsymbol{\theta}_j \mid \mathbf{x}_j, \hat{\mathcal{U}}, \hat{\boldsymbol{\pi}})$, in which $\hat{\mathcal{U}}, \hat{\boldsymbol{\pi}}$ denote the estimates returned by Algorithm 1. To test for significance, we use the local false sign rate (*lfsr*), which has been used in both univariate (Stephens, 2017; Xie and Stephens, 2022) and multivariate (Urbut et al., 2019; Liu et al., 2023; Zou et al., 2024) settings. The *lfsr* is defined as

$$(28) \quad \text{lfsr}_{j_r} := \min\{p_{\text{post}}(\theta_{j_r} \geq 0), p_{\text{post}}(\theta_{j_r} \leq 0)\}.$$

In particular, a small *lfsr* indicates high confidence in the sign of θ_{j_r} . The *lfsr* is robust to modeling assumptions, which is helpful for reducing sensitivity to the choice of prior (Stephens, 2017).

5. Numerical comparisons. We ran simulations to (i) compare the performance of the different approaches to updating the covariance matrices \mathbf{U}_k ; (ii) assess the benefits of the penalties and constraints; and (iii) assess the sensitivity of the results to the choice of K , the number of mixture components in the prior.

We used the Dynamic Statistical Comparisons software (<https://github.com/stephenslab/dsc>) to perform the simulations. Code implementing the simulations is provided in the supplementary ZIP file (Yang, Carbonetto and Stephens, 2024a), and includes a workflow website (Blischak, Carbonetto and Stephens, 2019) for browsing the results. The code and workflow website is also available online at <https://github.com/yunqiyang0215/udr-paper>.

5.1. *Data generation.* We simulated all data sets from the EBMNM model (1–2); that is, for each data set, we simulated the “true” means $\boldsymbol{\theta}_1, \dots, \boldsymbol{\theta}_n \in \mathbb{R}^R$ from the mixture prior (2) then we simulated observed data, the “noisy” means $\mathbf{x}_1, \dots, \mathbf{x}_n \in \mathbb{R}^R$, independently given the true means. Note that model fitting and inferences were performed using only $\mathbf{x}_1, \dots, \mathbf{x}_n$; the true means $\boldsymbol{\theta}_1, \dots, \boldsymbol{\theta}_n$ were only used to evaluate accuracy of the inferences. Further, to evaluate the ability of the model to generalize to other data, we also simulated test sets with true means $\boldsymbol{\theta}_1^{\text{test}}, \dots, \boldsymbol{\theta}_{n_{\text{test}}}^{\text{test}}$ and observed vectors $\mathbf{x}_1^{\text{test}}, \dots, \mathbf{x}_{n_{\text{test}}}^{\text{test}}$. These test sets were simulated in the same way as the training sets.

In all cases, we set the number of mixture components K to 10, with uniform mixture weights, $\pi_1, \dots, \pi_{10} = 1/10$. We generated the $K = 10$ covariance matrices $\mathbf{U}_1, \dots, \mathbf{U}_{10}$ in two different ways, which we refer to as the “hybrid” and “rank-1” scenarios:

1. **Hybrid scenario.** We used 3 canonical covariance matrices, and randomly generated an additional 7 covariance matrices randomly from an inverse-Wishart distribution with scale matrix $\mathbf{S} = 5\mathbf{I}_R$ and $\nu = R + 2$ degrees of freedom. The 3 canonical matrices were as follows: $\mathbf{U}_1 = 5\mathbf{e}_1\mathbf{e}_1^T$, a matrix of all zeros except for a 5 in the top-left position, which generates “singleton” mean vectors with a single non-zero element, $\boldsymbol{\theta}_j = (\theta_{j1}, 0, \dots, 0)$; $\mathbf{U}_2 = 5\mathbf{1}\mathbf{1}^T$, which generates equal means $\boldsymbol{\theta}_j = (\alpha_j, \dots, \alpha_j)$ for some scalar α_j ; and $\mathbf{U}_3 = 5\mathbf{I}_R$, which generates mean vectors $\boldsymbol{\theta}_j$ that are independent in each dimension.
2. **Rank-1 scenario.** We used 5 covariance matrices of the form $\mathbf{U}_k = 5\mathbf{e}_k\mathbf{e}_k^T$, $k = 1, \dots, 5$, which generate mean vectors of length R with zeros everywhere except at the k th position. The remaining 5 covariances were random rank-1 matrices of the form $\mathbf{U}_k = \mathbf{u}_k\mathbf{u}_k^T$, $\mathbf{u}_k \sim N_R(\mathbf{0}, \mathbf{I}_R)$, $k = 6, \dots, 10$.

In both scenarios, we simulated large, low-dimension data sets ($n = 10,000$, $R = 5$), and smaller, high-dimension data sets ($n = 1,000$, $R = 50$). We refer to these data sets as “large n/R ” and “small n/R ”, respectively. To allow comparisons between TED, ED and FA, in all cases we simulated data sets with homoskedastic errors; that is, $\mathbf{V}_j = \mathbf{I}_R$, $j = 1, \dots, n$ and $\mathbf{V}_j^{\text{test}} = \mathbf{I}_R$, $j = 1, \dots, n_{\text{test}}$.

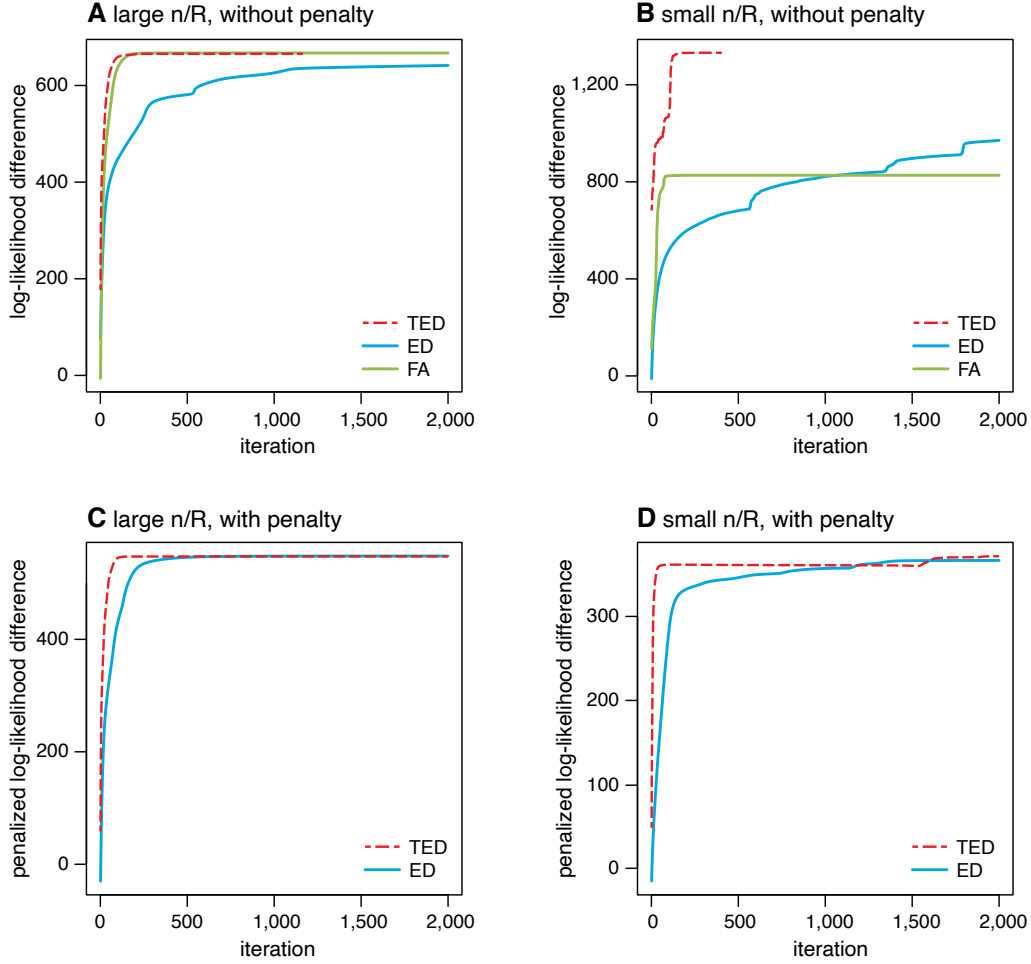


FIG 1. Illustrative examples comparing convergence of TED, ED and FA. Each plot shows the algorithms’ progress over iterations on a single simulated data set. A and C show the results for the same data set, and similarly for B and D. In all cases, we ran 2,000 iterations, although in some cases, TED updates stopped early because the updates converged to a stationary point of the objective (the likelihood or the penalized likelihood). For examples A and B, no penalty was used; for examples C and D, the inverse Wishart (IW) penalty was used with penalty strength $\lambda = R$. Log-likelihood and penalized log-likelihood differences are plotted with respect to the (penalized) log-likelihood near the initial estimate. An initial round of 20 ED iterations common to all the runs (the “warm start”) is not shown in these plots.

5.2. Results.

5.2.1. Comparison of convergence. We first focused on comparing the convergence of the different updates (TED, ED and FA). For brevity, we write “TED” as shorthand for “the algorithm with TED updates”, and similarly for ED and FA. To compare the updates under the same conditions, we used FA here to fit full-rank covariance matrices, not rank-1 matrices. We ran TED and ED with and without the IW penalty.

We ran all methods on 100 “large n/R ” data sets and 100 “small n/R ” data sets simulated in the hybrid scenario, setting $K = 10$ to match the simulated truth. To reduce the likelihood that the different updates converge to different local solutions, we performed a prefitting stage in which we ran 20 iterations of ED from a random initial starting point (specifically, the initialization was $\pi_k = 1/10$, $s_k = 1$, with randomly generated U_k , $k = 1, \dots, 10$). We call this a “warm start”. We then ran each algorithm for at most 2,000 iterations after this

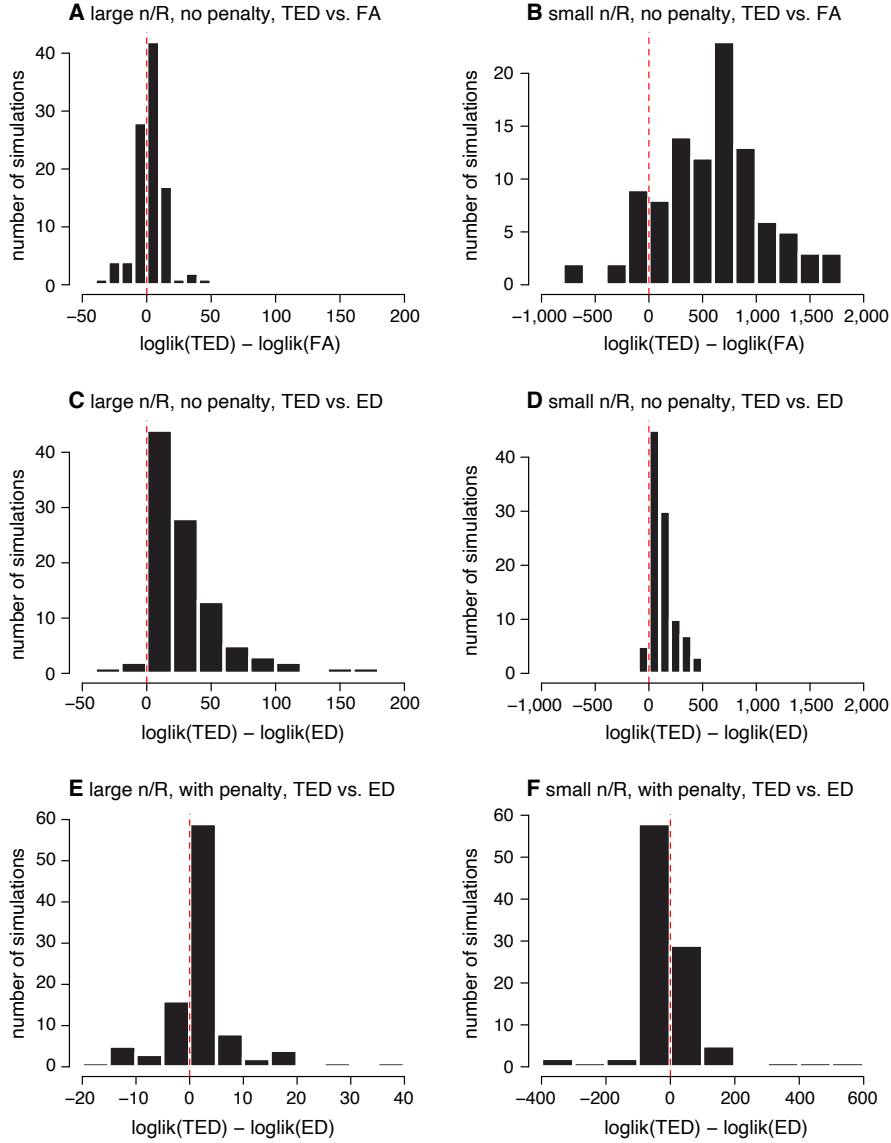


FIG 2. Comparison of convergence of TED, ED and FA. Each plot summarizes the results from 100 simulations. In each simulation, log-likelihood achieved after (at most) 2,000 iterations was recorded. Panels E and F show differences in the penalized log-likelihoods (IW penalty, $\lambda = R$).

warm start. Figure 1 shows illustrative results for two data sets (one large n/R and one small n/R), and Figure 2 summarizes the results across all simulations.

The results in Figure 1 illustrate typical behavior. Among the unpenalized updates, TED and FA converged much more quickly than ED. For the penalized updates, TED still converged more quickly than ED, but the difference is less striking than without the penalty. In the small n/R example the three methods appear to have converged to different solutions (despite the use of a warm start). This is not unexpected due to the non-convexity of the objective function, and illustrates an important general point to keep in mind: improvements in the quality of solution obtained may be due to either faster convergence to the solution, convergence to a local solution with higher objective, or both.

The results in Figure 2 confirm that some of the patterns observed in the illustrative example are true more generally. In the unpenalized case (Panels A–D), TED often arrived at a

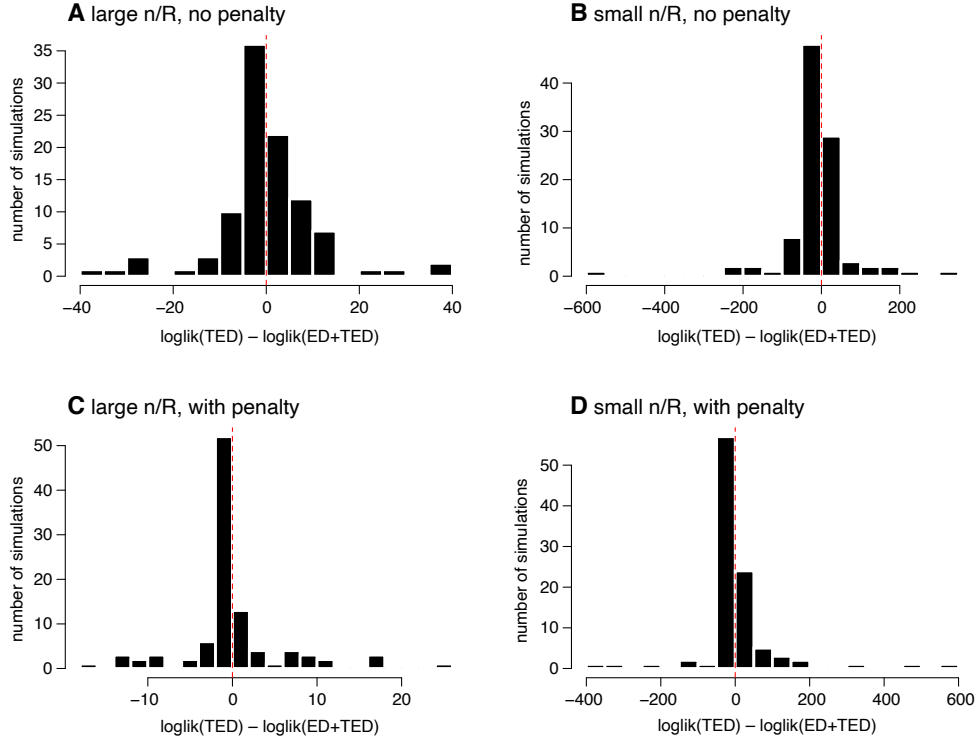


FIG 3. Results demonstrating the ability of TED to “rescue” ED. The log-likelihood or penalized log-likelihood obtained by performing at most 2,000 TED updates is compared against performing 2,000 iterations of ED, followed by another round of (at most) 2,000 iterations of TED updates (“ED+TED”). Each plot summarizes the results from 100 simulations, the same simulations as in Figure 2.

better solution than FA or ED, although in the large n/R setting FA was comparable to TED (Panel A). In the penalized case, the TED and ED solutions were much more similar for both large and small n/R (Panels E, F).

The improved performance of (unpenalized) TED vs. ED could be due either to faster convergence (e.g., Figure 1A) or due to convergence to a better local optimum (e.g., Figure 1B). To investigate this, we assessed whether TED can “rescue” ED by running TED initialized to the ED solution (“ED+TED”). If ED converges to a poorer local optimum, then TED will not rescue it, and ED+TED will be similar to ED; on the other hand, if ED is simply slow to converge, then ED+TED will be similar to TED. The results in Figure 3 show that TED usually rescues ED; the ED+TED estimates were consistently very similar to the TED estimates, regardless of whether a penalty was used or not. This suggests that the improved performance of TED is generally due to faster convergence.

To assess how additional iterations improve ED’s performance, we reran ED for 100,000 iterations instead of only 2,000. Since these runs take a long time, we examined only a few simulated data sets randomly selected from the large n/R and small n/R scenarios (Supplementary Figure 1). Even after 100,000 iterations, ED fell measurably short of 1,000 updates of TED (average difference of 40.6 log-likelihood units).

In summary, our experiments confirm that, for homoskedastic errors (which is the setting where all three methods apply), TED exhibited the best performance. This is not unexpected since TED solves the subproblem (eq. 25 or 27) exactly whereas ED and FA do not. Our experiments also show that including a penalty can help improve convergence behavior, especially for ED. Thus, including the penalty has computational benefits in addition to statistical benefits demonstrated below.

5.2.2. *Comparison of the penalties and constraints.* Next we evaluated the benefits of different penalties and constraints for estimation and significance testing of the underlying means θ_j . We focused on TED and ED with and without penalties, and on fitting rank-1 matrices using TED. (Since TED solves the subproblem exactly, rather than iteratively, TED should be better than FA in this setting with homoskedastic variances. The main benefit of FA is that it can fit rank-1 matrices with heteroskedastic variances.)

We compared methods using the following evaluation measures:

- **Plots of power vs. false sign rate (FSR).** These plots are similar to the more commonly-used plots of “power vs. false discovery rate,” but improve robustness and generality by requiring “true discoveries” to have the correct sign. The better methods are those that achieve higher power at a given FSR. See the Supplementary Text (Yang, Carbonetto and Stephens, 2024b) for definitions.
- **Empirical False Sign Rate (FSR).** We report the empirical FSR among tests that were significant at $lfsr < 0.05$. A well-behaved method should have a small empirical FSR, certainly smaller than 0.05. We consider an FSR exceeding 0.05 to be indicative of a poorly behaved method.
- **Accuracy of predictive distribution.** To assess generalizability of the estimates of \mathcal{U} and π , we compared the marginal predictive density (3) in test samples, $p(\mathbf{x}_j^{\text{test}} | \hat{\mathcal{U}}, \hat{\pi}, \mathbf{V}_j^{\text{test}})$, against the “ground-truth” marginal predictive density $p(\mathbf{x}_j^{\text{test}} | \mathcal{U}^{\text{true}}, \pi^{\text{true}}, \mathbf{V}_j^{\text{test}})$, where $\mathcal{U}^{\text{true}}, \pi^{\text{true}}$ denote the parameters used to simulate the data. We summarized the relative accuracy in the predictions as

$$(29) \quad \frac{1}{n_{\text{test}}} \sum_{j=1}^{n_{\text{test}}} \log \left\{ \frac{p(\mathbf{x}_j^{\text{test}} | \mathcal{U}^{\text{true}}, \pi^{\text{true}})}{p(\mathbf{x}_j^{\text{test}} | \hat{\mathcal{U}}, \hat{\pi})} \right\}.$$

This measure can be interpreted as (an approximation of) the Kullback-Leibler (K-L) divergence from the true predictive distribution to the estimated predictive distribution. Smaller K-L divergences are better.

We simulated 20 data sets with large n/R and another 20 data sets with small n/R under both the hybrid and rank-1 scenarios (80 data sets in total). In all cases, model fitting was performed as above, again with $K = 10$. The results are summarized in Figures 4 and 5. In all comparisons, we included results from the “oracle” EBMNM model—that is, the model used to simulate the data—as a point of reference.

Results for the hybrid setting are shown in Figure 4. The results show a clear benefit of using a penalty in the small n/R setting: both IW and NN penalties improved the power vs. FSR and the accuracy of predictive distributions. For large n/R data sets, the penalties do not provide a clear benefit, but also do not hurt performance. In both cases TED and ED perform similarly, suggesting that the poor convergence of ED observed in previous comparisons may have less impact on performance than might have been expected. The rank-1 constraints performed very poorly in all tasks, which is perhaps unsurprising since the true covariances were (mostly) not rank-1.

Results for the rank-1 scenario are shown in Figure 5. In this case, imposing rank-1 constraints on the covariance matrices improved predictive performance—which makes sense because the true covariances were indeed rank-1—but produced worse performance in other metrics. In particular, the $lfsr$ values from the rank-1 constraint are very poorly calibrated. This is because, as noted in Liu et al. (2023), the rank-1 constraint leads to $lfsr$ values that do not differ across conditions; see the Discussion (Section 7) for more on this. Penalized estimation of the covariance matrices (using either a IW or NN penalty) consistently achieved

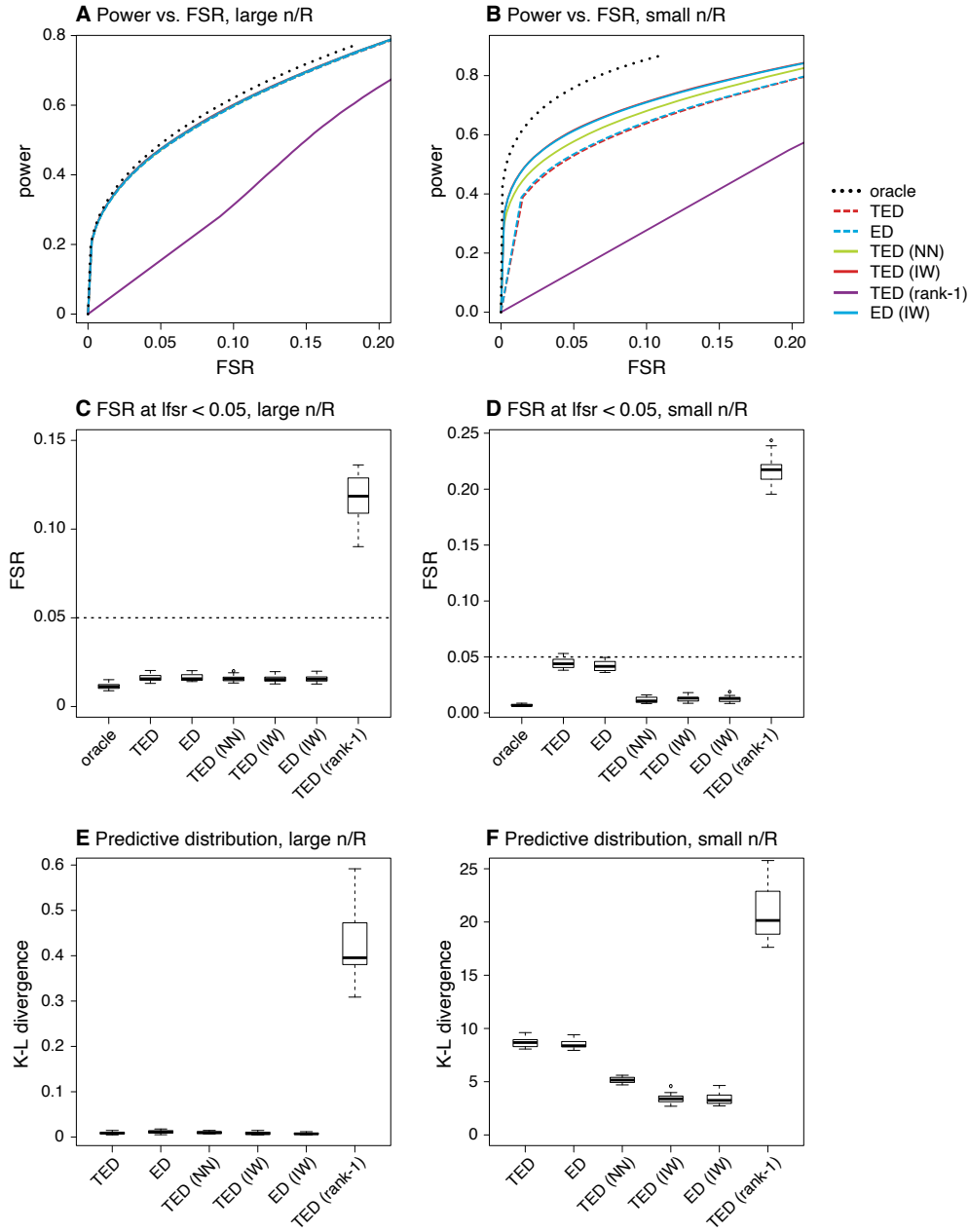


FIG 4. Comparison of penalties, constraints and updates (ED vs. TED) in the “hybrid” simulated data sets. For the IW and NN penalties, the penalty strength was set to $\lambda = R$. In C and D, the target FSR is shown as a dotted horizontal line at 0.05. In A, most of the methods are not visible because the lines overlap at the top near the oracle result. Note that the oracle model always achieves a K-L divergence of zero.

the best power at a given FSR in both the large n/R and small n/R settings. Interestingly, (unpenalized) TED performed much worse than (unpenalized) ED in the power vs. FSR for large n/R . We speculate that this was due to the slow convergence of ED providing sort of “implicit regularization”. However, explicit regularization via a penalty seems preferable to implicit regularization via a poorly converging algorithm, and overall penalized estimation was the winning (or equally winning) strategy across a variety of settings.

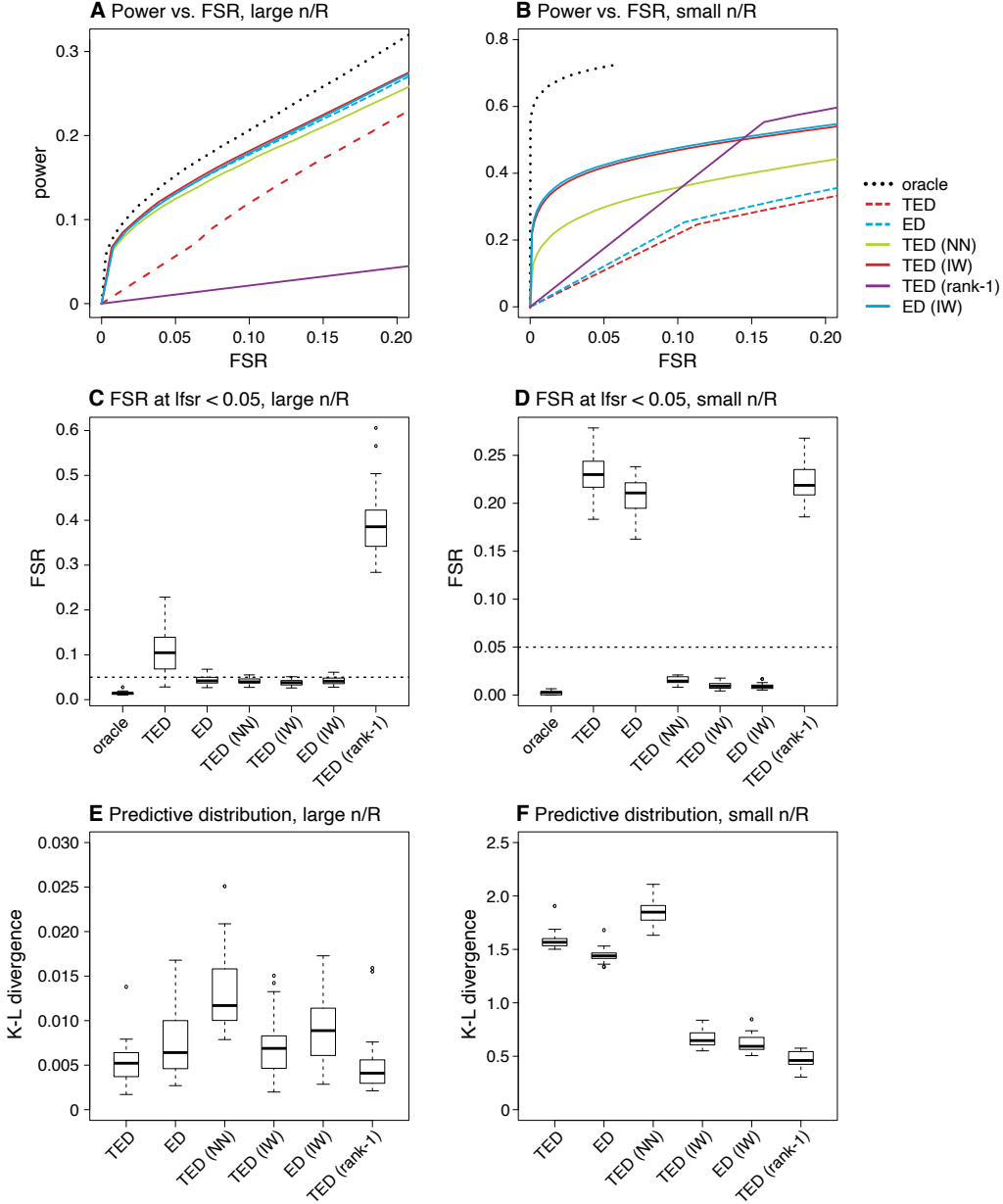


FIG 5. Comparison of penalties, constraints and updates (ED vs. TED) in the “rank-1” simulated data sets. For the IW and NN penalties, the penalty strength was set to $\lambda = R$. In C and D, the target FSR is shown as a dotted horizontal line at 0.05. Note that the oracle model always achieves a K-L divergence of zero.

5.2.3. Robustness to mis-specifying the number of mixture components. In the above experiments, we fit all models with a value of K that matched the model used to simulate the data. In practice, however, K is unknown, and so we must also consider situations in which K is mis-specified. Intuitively, one might expect that overstating K may lead to overfitting and worse performance; [Urbut et al. \(2019\)](#) argued however that the use of the mixture components centered at zero in the prior (2) makes it robust to overfitting because the mean-zero constraint limits their flexibility. Here we assess this claim.

In these experiments, we analyzed the same 80 data sets as in the previous section (simulated with $K = 10$). We fit models with different penalties, constraints and algorithms, with

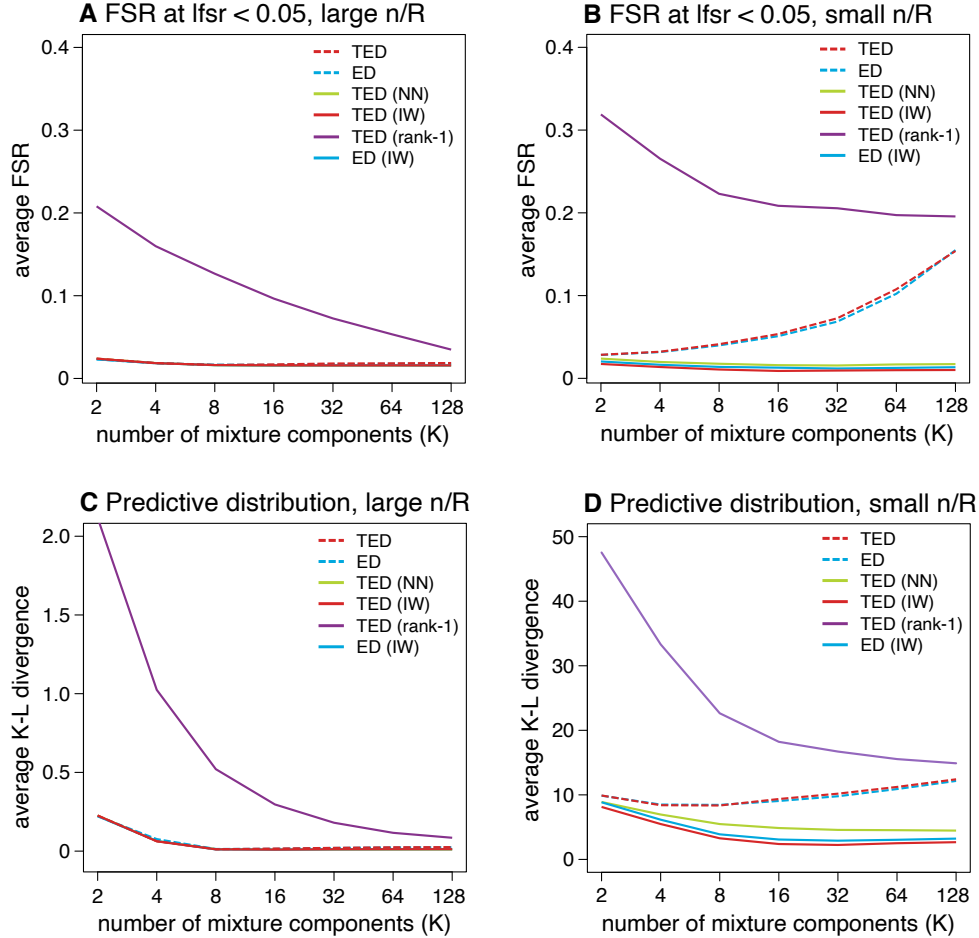


FIG 6. Assessment of robustness to mis-specifying K in “hybrid” simulated data sets. All results are averages over 20 data sets, each simulated with $K = 10$ mixture components. In A and C, most of the methods are not visible because they overlap with the “TED-IW” result.

K varying from 2 to 128. We compared results in both the accuracy of the predictive distribution (K-L divergence) and the average FSR at an $lfsr$ threshold of 0.05.

Results are shown in Figures 6 and 7. For large n/R , all model fits except those with the rank-1 constraints were robust to overstating K , with similarly good performance even at $K = 128$. This is generally consistent with the claim in [Urbut et al. \(2019\)](#) that the mixture prior should be robust to overstating K . However, for small n/R the story is quite different: all of the unpenalized algorithms eventually showed a decline in performance when K was too large, presumably due to “overfitting”. In comparison, all the penalized methods were more robust to overstating K ; the performance did not substantially decline as K increased.

The improved robustness of the penalized methods could be achieved in at least two different ways: they could be using a smaller number of components by estimating some of the mixture weights π_k to be very small; or by estimating some of the components k to have very similar covariances U_k (or both). To investigate these explanations, we looked at the models with $K = 100$ components and recorded the number of “important” components, defined as components k with $\pi_k > 0.01$. We found that the penalized methods tended to produce much fewer “important” components than the unpenalized methods (Supplementary Figure 4). Essentially, the penalties have the effect of shrinking each U_k toward the identity matrix, so a component is assigned a small weight whenever the identity matrix does not match the truth.

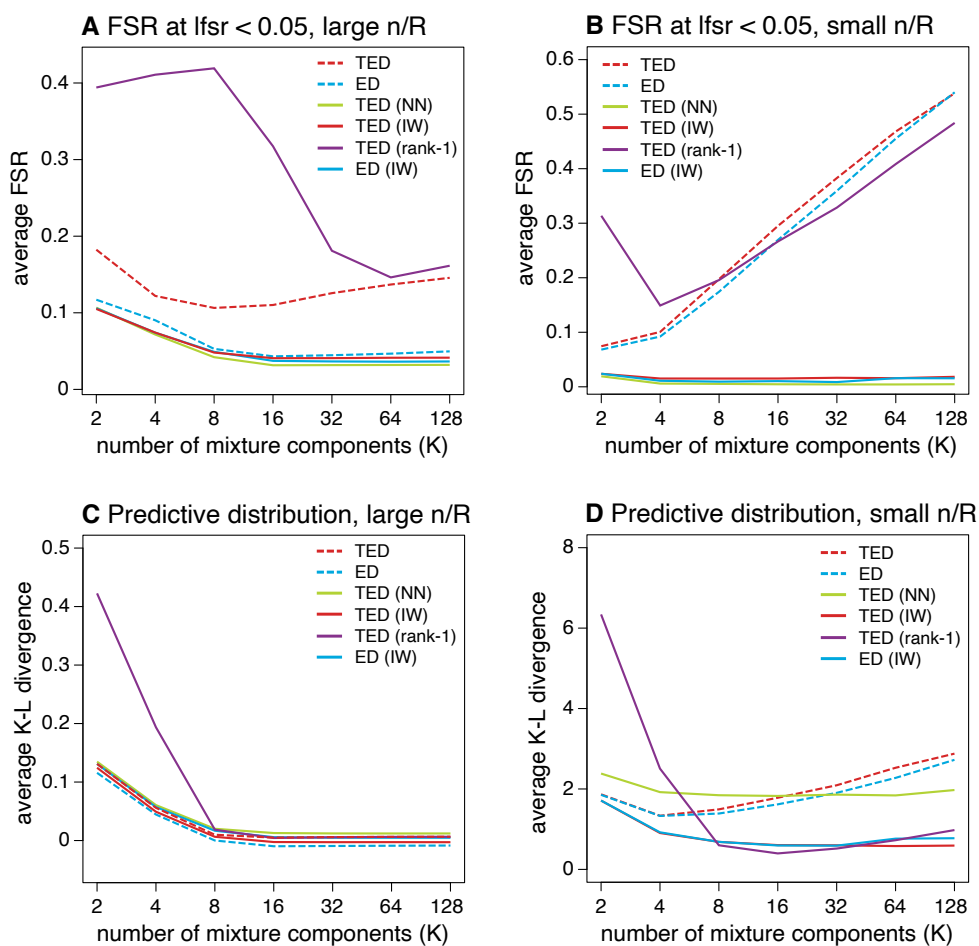


FIG 7. Assessment of robustness to mis-specifying K in “rank-1” simulated data sets. All the results shown in the plots are averages over the 20 data sets. All data sets were simulated with $K = 10$ mixture components.

In summary, our results support the use of penalized methods with a large value of K as a simple and robust way to achieve good performance in different settings.

6. Analysis of genetic effects on gene expression in 49 human tissues. To illustrate our methods on real data, we used the EBMNM model to analyze the effects of genetic variants on gene expression (“*cis*-eQTLs”) in multiple tissues. The use of the EBMNM model for this purpose was first demonstrated in [Urbut et al. \(2019\)](#). They used a two-stage procedure to fit the EBMNM models: (i) fit the EBMNM model to a subset of “strong” eQTLs to estimate the prior covariance matrices; and (ii) fit a (modified) EBMNM model to all eQTLs—or a random subset of eQTLs—using the covariance matrices from (i). The model from (ii) was then used to perform inferences and to test for eQTLs in each tissue. Our new methods are relevant to (i), and so we focus on stage (i) here. For (i), [Urbut et al. \(2019\)](#) used the ED algorithm without a penalty. Recognizing that the results are sensitive to initialization, they described a detailed initialization procedure.¹ We coded an initialization procedure similar to this, which we refer to as the “specialized initialization”. We note that the specialized

¹An updated version of the initialization procedure of [Urbut et al. \(2019\)](#) is described in the “flash_mash” vignette included in the mashr R package. See also https://stephenslab.github.io/mashr/articles/flash_mash.html.

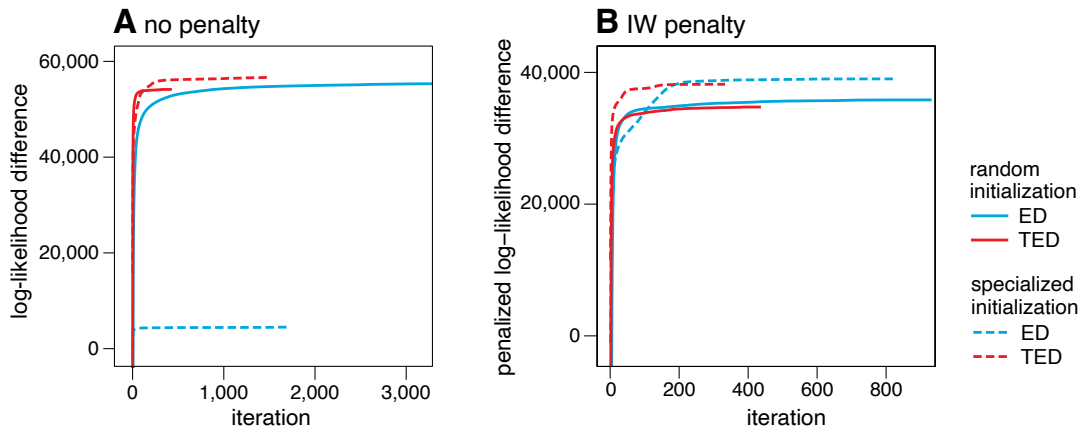


FIG 8. Plots showing improvement in model fit over time for the GTEx data, using different initialization schemes, different prior covariance matrix updates, and penalty vs. no penalty (maximum-likelihood). Log-likelihood differences and penalized log-likelihood differences are with respect to the (penalized) log-likelihood near the initial estimate. All models were fit with $K = 40$ mixture components. In B, the inverse wishart (IW) penalty was used with penalty parameter $\lambda = R$. In all cases, the model fitting was halted when the difference in the log-likelihood between two successive updates was less than 0.01, or when 5,000 updates were performed, whichever came first.

initialization adds substantially to both the complexity and computation time of the overall fitting procedure. Our goal was to assess the benefits of different EBMNM analysis pipelines which consisted of combinations of: TED vs. ED updates; specialized initialization vs. a simple random initialization; and penalty vs. no penalty (maximum-likelihood). All these combinations resulted in 8 different analyses of multi-tissue cis-eQTL data.

We analyzed z -scores from tests for association between gene expression in dozen human tissues and genotypes at thousands of genetic variants. The z -scores came from running the “Matrix eQTL” software (Shabalin, 2012) on genotype and gene expression data in release 8 of the Genotype-Tissue Expression (GTEx) Project (GTEx Consortium, 2020). Following Urbut et al. (2019), we selected the genetic variants with the largest z -score (in magnitude) across tissues for each gene. After data filtering steps, we ended up with a data set of z -scores for $n = 15,636$ genes and $R = 49$ tissues. We fit the EBMNM model to these data, with all the V_j set to a common correlation matrix; that is, $V_j = C$, where C is a correlation matrix of non-genetic effects on expression. This correlation matrix C was estimated from the association test z -scores following the approach described in Urbut et al. (2019). In all runs, we set $K = 40$ to match the number of covariance matrices produced by our specialized initialization. And, in all cases, we initialized the mixture weights to $\pi_k = 1/40$ and the scaling factors (when needed) to $s_k = 1$. The supplementary ZIP file (Yang, Carbonetto and Stephens, 2024a) contains the code and data implementing these analyses as well as the results we generated.

Figure 8 shows the improvement of the model fits over time in the 8 different analyses. In the analyses without a penalty (A), the TED updates with a specialized initialization produced the best fit, while the ED and TED updates with random initialization were somewhat worse (e.g., TED with random initialization produced a fit that was 2,497.78 log-likelihood units worse, or 0.16 log-likelihood units per gene). Strikingly, the ED updates with specialized initialization resulted in a much worse fit. We attribute this to the fact that the specialized initialization includes many rank-1 matrices, and the “subspace preserving” property of the ED updates means that these matrices are fixed at their initialization (they changed only by a scaling factor), which substantially limits their ability to adapt to the data. In the penalized case, consistent with our simulation results, there was less difference between ED vs. TED.

TABLE 2

Cross-validation results on the GTEx data. The “mean relative log-likelihood” column gives the increase in the test-set log-likelihood over the worst log-likelihood among the 8 approaches compared, divided by total number of genes in each test set. The “average number of iterations” column gives the number of iterations performed until the stopping criterion is met (log-likelihood between two successive updates less than 0.01, up to a maximum of 5,000 iterations), averaged over the 5 CV folds.

initialization	algorithm	penalty	mean relative log-likelihood	average number of iterations
specialized	ED	none	0.00	1,101
specialized	ED	IW	1.21	1,083
specialized	TED	none	0.88	1,054
specialized	TED	IW	1.19	412
random	ED	none	0.25	5,000
random	ED	IW	0.86	1,377
random	TED	none	0.20	450
random	TED	IW	0.94	584

In both cases, the specialized initialization improved the fit relative to random initialization (e.g., TED increased the penalized log-likelihood by 3,176, or about 0.2 per gene). Note that adding a penalty function makes the subspace preserving property of the ED updates irrelevant by forcing the matrices to be full rank.

To compare the quality of the fits obtained by each method, we computed log-likelihoods on held-out (“test set”) data, using a 5-fold cross-validation (CV) design. Following the usual CV setup, in each CV fold 80% of the genes were in the training set, and the remaining 20% were in the test set. Then we fit an EBMNM model to the training set following each of the 8 approaches described above, and measured the quality of the fit by computing the log-likelihood in the test set. We also recorded the number of iterations. Within a given fold, the number of components K was the same across all the analyses, and was set depending on the number of covariance matrices produced by the specialized initialization. (K was at least 32 and at most 39.)

Consistent with the simulations, the inclusion of a penalty consistently improved the test set log-likelihood (Table 2). With a penalty, the specialized initialization also improved the test set log-likelihood compared with a random initialization. Of the 8 approaches tried, the one used by [Urbut et al. \(2019\)](#)—ED with no penalty and specialized initialization—resulted in the worst test-set likelihood.

Although the analyses with a specialized initialization resulted in better fits than the analyses with a random initialization, the specialized initialization also had substantial computational overhead; running the initialization procedures on these data took more than 1 hour (by comparison, running a single iteration of the EBMNM algorithm typically took about 1 second). Therefore, on balance, one might prefer to dispense with the specialized initialization. Based on these results and considerations, we subsequently examined in more detail the analysis with ED, no penalty and specialized initialization—which was the approach used in [Urbut et al. \(2019\)](#)—and the analysis with TED, IW penalty and random initialization. For brevity, we refer to these analyses as the “previous pipeline” and “new pipeline”, respectively.

A notable outcome of the new pipeline is that it produced a prior with weights that were more evenly distributed across the mixture components (Figure 9). For example, the new pipeline produced 22 covariances with weights greater than 1%, whereas the previous pipeline produced only 10 covariances with weights more than 1%. Also, the top 16 covariances accounted for 85% of the total weight in the new pipeline, whereas only 6 covariances were needed to equal 85% total weight in the previous pipeline. Inspecting the individual covariances generated from the two analysis pipelines, there many strong similarities in the estimated sharing patterns (Figures 10 and 11). But the new analysis pipeline

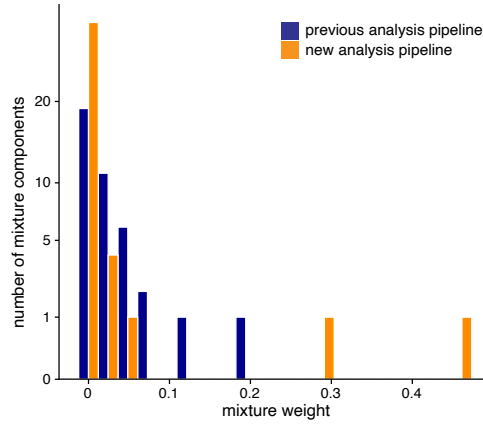


FIG 9. Comparison of the prior mixture weights π from the previous pipeline vs. the new pipeline. The histogram shows the distributions of the $K=40$ prior mixture weights resulting from both pipelines.

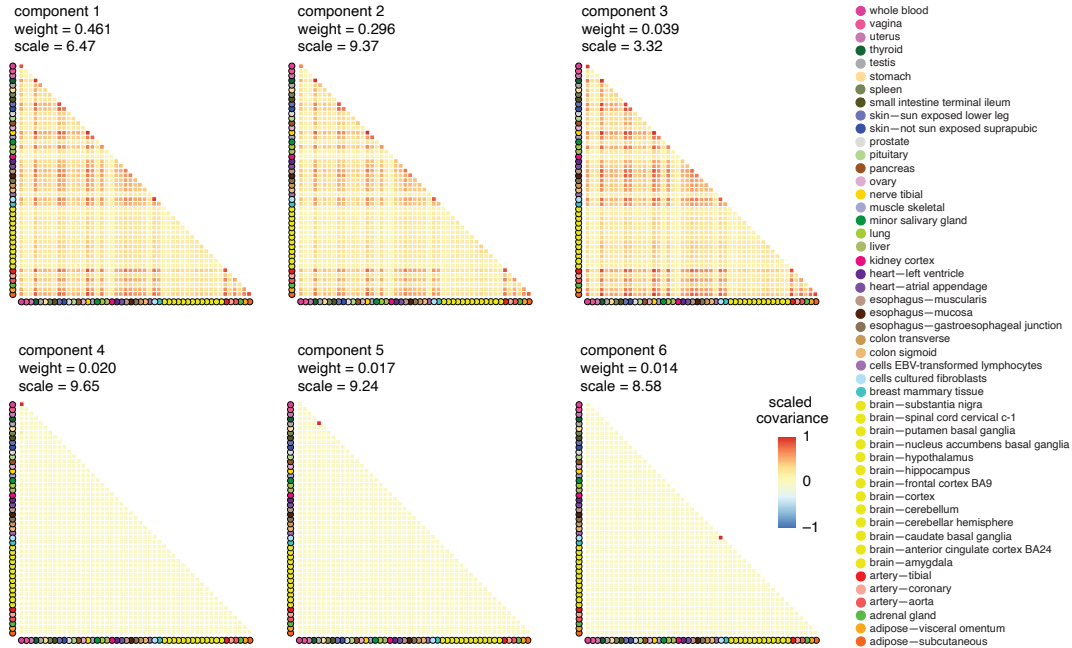


FIG 10. Top effect-sharing patterns in the EBMNM model fit to the GTEx data using the previous pipeline. The “top” patterns are the mixture components with the largest weights. Each heatmap shows the 49×49 scaled covariance matrix U_k/σ_k^2 , where σ_k^2 is the largest diagonal element of U_k , so that all elements of the scaled covariance lie between -1 and 1 . (The vast majority of the covariances are positive; negative correlations are unexpected.) The scaled covariance matrices are arranged in decreasing order by mixture weight. The “scale” above each heatmap is σ_k . Note that the top three covariance matrices capture broadly similar effect-sharing patterns, but different effect scales.

learned a greater variety of tissue-specific patterns (e.g., whole blood, testis, thyroid) and tissue-sharing patterns, many of which appear to reflect underlying tissue biology. For example, sharing pattern 6 (see Figure 11) captures sharing of brain-specific effects (including the pituitary gland, which is found at the base of the brain near the hypothalamus). Sharing pattern 8 may reflect the fact that skin and the mucosa layer of the esophagus wall both contain squamous epithelial cells. Additionally, we looked at more closely at the 8 genes with

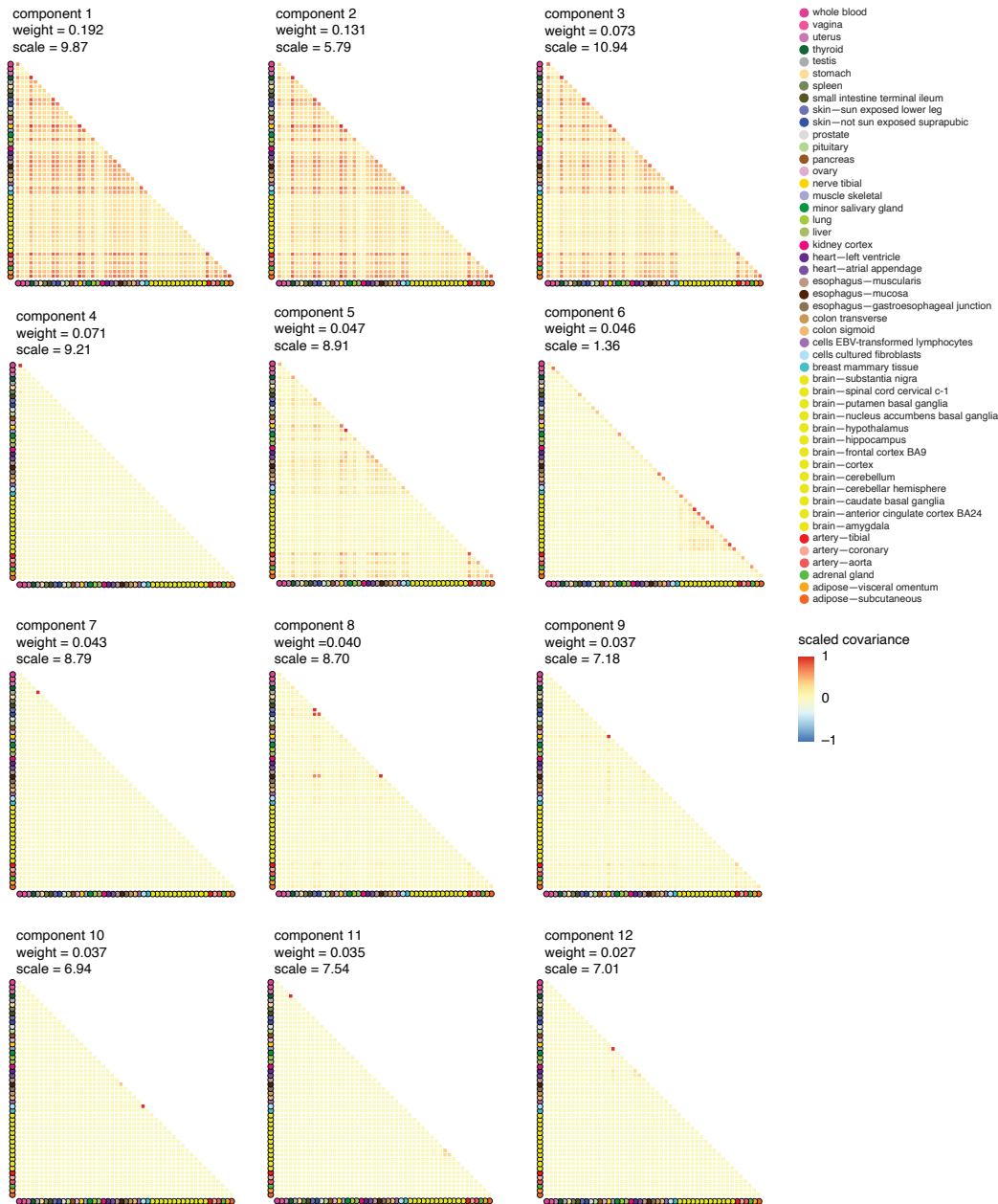


FIG 11. Top effect-sharing patterns in the GTEx data generated by the new analysis pipeline. See the caption to Fig. 10 for more details.

very strong posterior weights (>98%) on component 6, the component capturing eQTL sharing among brain tissues: *HOMER1*, *JPT1*, *SRSF2*, *ABCA1*, *GPATCH8*, *SYNGAP1*, *SPI1* and *LGDN*. Several of these have been linked to neurological and neuropsychiatric conditions, including major depression, schizophrenia, attention dementia and Alzheimer's disease. For example, *SYNGAP1* is linked to neuronal functions and psychiatric diseases based on results from the GWAS Catalog (Sollis et al., 2022) and from functional studies (Jeyabalan and Clement, 2016; Llamosas et al., 2020). In summary, the improvements to the EBMNM analysis pipeline should result in the discovery of a greater variety of cross-tissue genetic effects on gene expression.

7. Discussion. The growing interest in deciphering shared underlying biological mechanisms has led to a surge in multivariate analyses in genomics; among the many recent examples are multi-trait analyses (Wu et al., 2020; Luo et al., 2020) and multi-ancestry analyses to improve polygenic risk scores (Zhang et al., 2023). The EBMNM approach described here and in Urbut et al. (2019) provide a versatile and robust multivariate approach to multivariate analysis. We have implemented and compared several algorithms for this problem. These algorithms not only enhance accuracy but also provide a level of flexibility not achieved by other methods.

One of our important findings is that using low-rank covariance matrices in this setting, as was done in Urbut et al. (2019), is not recommended. In particular, while low-rank matrices may be relatively easy to interpret, they lead to poorly calibrated *lfsr* values (e.g., Figure 5). For intuition, consider fitting a EBMNM model with $K = 1$ and a rank-1 covariance matrix, $U_1 = \mathbf{u}\mathbf{u}^T$. (We credit Dongyue Xie for this example.) Under this model, the mean is $\boldsymbol{\theta}_j = \mathbf{u}a_j$ for some a_j , and therefore, given a \mathbf{u} , the signs of all the elements of $\boldsymbol{\theta}_j$ are fully determined by a_j . As a result, all elements of $\boldsymbol{\theta}_j$ will have the same *lfsr*, and so this model cannot capture situations where one is confident in the sign of some elements of $\boldsymbol{\theta}_j$ but not others. This can cause problems *even if the model is correct*, that is, when the true covariances are rank-1, as in Figure 5. There are some possible ways to address these issues, say, by imposing sparsity on estimates of \mathbf{u} , and this could be an area for future work.

Even when the pitfalls of low-rank matrices are avoided, it is still the case that EB methods tend to understate uncertainty compared to “fully Bayesian” methods (e.g., Morris 1983; Wang and Titterton 2005). As a result, one should expect that the estimated *lfsr* values may be anti-conservative; that is, the *lfsr* values are smaller than they should be. Indeed, we saw this anti-conservative behavior across many of our simulations and methods (Supplementary Figures 2 and 3). For this reason estimated *lfsr* rates should be treated with caution, and it would be prudent to use more stringent significance thresholds than are actually desired (e.g., an *lfsr* threshold of 0.01 rather than 0.05). In the special case where $\mathbf{V} = \mathbf{I}$, it should be possible to improve calibration of significance tests by using ideas from Lei and Fithian (2018). Improving calibration in the general case of dependent multivariate tests seems to be an important area for future research.

Acknowledgments. We thank Gao Wang and Sarah Kim-Hellmuth for their help in preparing the GTEx data. We thank Yuxin Zou, Yusha Liu and Dongyue Xie for helpful discussions on MASH and the mashr software. And we thank the staff at the Research Computing Center at the University of Chicago for maintaining the computing resources used in our numerical experiments.

Funding. This work was supported by NIH grant R01HG002585 to MS.

SUPPLEMENTARY MATERIAL

Supplementary materials

The supplementary PDF includes supporting mathematical results and additional tables and figures.

R package and code reproducing the analyses

ZIP file containing the source code for the R package as well as the source code reproducing the results of the simulations and analysis of the GTEx data.

REFERENCES

- ARAUJO, D. S., NGUYEN, C., HU, X., MIKHAYLOVA, A. V., GIGNOUX, C., ARDLIE, K. et al. (2023). Multivariate adaptive shrinkage improves cross-population transcriptome prediction and association studies in underrepresented populations. *Human Genetics and Genomics Advances* **4** 100216.
- BARBEIRA, A. N., MELIA, O. J., LIANG, Y., BONAZZOLA, R., WANG, G., WHEELER, H. E., AGUET, F., ARDLIE, K. G., WEN, X. and IM, H. K. (2020). Fine-mapping and QTL tissue-sharing information improves the reliability of causal gene identification. *Genetic Epidemiology* **44** 854–867.
- BHADRA, A., DATTA, J., POLSON, N. G. and WILLARD, B. (2019). Lasso meets horseshoe: a survey. *Statistical Science* **34** 405–427.
- BLISCHAK, J. D., CARBONETTO, P. and STEPHENS, M. (2019). Creating and sharing reproducible research code the workflow way [version 1; peer review: 3 approved]. *F1000Research* **8**.
- BONDER, M. J., SMAIL, C., GLOUDEMANS, M. J., FRÉSARD, L., JAKUBOSKY, D., D’ANTONIO, M. et al. (2021). Identification of rare and common regulatory variants in pluripotent cells using population-scale transcriptomics. *Nature Genetics* **53** 313–321.
- BOVY, J., HOGG, D. W. and ROWEIS, S. T. (2011). Extreme Deconvolution: Inferring complete distribution functions from noisy, heterogeneous and incomplete observations. *Annals of Applied Statistics* **5** 1657–1677.
- CAI, T. and LIU, W. (2011). Adaptive thresholding for sparse covariance matrix estimation. *Journal of the American Statistical Association* **106** 672–684.
- CHI, E. C. and LANGE, K. (2014). Stable estimation of a covariance matrix guided by nuclear norm penalties. *Computational statistics and Data Analysis* **80** 117–128.
- GTEX CONSORTIUM (2020). The GTEx Consortium atlas of genetic regulatory effects across human tissues. *Science* **369** 1318–1330.
- GTEX CONSORTIUM, ARDLIE, K. G., DELUCA, D. S., SEGRÈ, A. V., SULLIVAN, T. J., YOUNG, T. R., GELFAND, E. T., TROWBRIDGE, C. A., MALLER, J. B., TUKIAINEN, T. et al. (2015). The Genotype-Tissue Expression (GTEx) pilot analysis: multitissue gene regulation in humans. *Science* **348** 648–660.
- DEMPSTER, A. P., LAIRD, N. M. and RUBIN, D. B. (1977). Maximum likelihood from incomplete data via the EM algorithm. *Journal of the Royal Statistical Society, Series B* **39** 1–22.
- EFRON, B. and MORRIS, C. (1972). Limiting the risk of Bayes and empirical Bayes estimators—Part II: the empirical Bayes case. *Journal of the American Statistical Association* **67** 130–139.
- FAN, J., LIAO, Y. and LIU, H. (2016). An overview of the estimation of large covariance and precision matrices. *Econometrics Journal* **19** C1–C32.
- FLUTRE, T., WEN, X., PRITCHARD, J. and STEPHENS, M. (2013). A statistical framework for joint eQTL analysis in multiple tissues. *PLoS Genetics* **9** e1003486.
- FRALEY, C. and RAFTERY, A. E. (2007). Bayesian regularization for normal mixture estimation and model-based clustering. *Journal of Classification* **24** 155–181.
- FRIEDMAN, J., HASTIE, T. and TIBSHIRANI, R. (2008). Sparse inverse covariance estimation with the graphical lasso. *Biostatistics* **9** 432–441.
- GHAHRAMANI, Z. and HINTON, G. E. (1996). The EM algorithm for mixtures of factor analyzers. Technical Report, University of Toronto.
- HAN, B. and ESKIN, E. (2011). Random-effects model aimed at discovering associations in meta-analysis of genome-wide association studies. *American Journal of Human Genetics* **88** 586–598.
- JEYABALAN, N. and CLEMENT, J. P. (2016). SYNGAP1: mind the gap. *Frontiers in Cellular Neuroscience* **10** 32.
- JOHNSTONE, I. (2019). Gaussian estimation: sequence and wavelet models. Available at https://imjohnstone.su.domains/GE_08_09_17.pdf.
- JOHNSTONE, I. M. and PAUL, D. (2018). PCA in high dimensions: an orientation. *Proceedings of the IEEE* **106** 1277–1292.
- KIM, Y., CARBONETTO, P., STEPHENS, M. and ANITESCU, M. (2020). A fast algorithm for maximum likelihood estimation of mixture proportions using sequential quadratic programming. *Journal of Computational and Graphical Statistics* **29** 261–273.
- LEDOIT, O. and WOLF, M. (2004). A well-conditioned estimator for large-dimensional covariance matrices. *Journal of Multivariate Analysis* **88** 365–411.
- LEDOIT, O. and WOLF, M. (2022). The power of (non-)linear shrinking: a review and guide to covariance matrix estimation. *Journal of Financial Econometrics* **20** 187–218.
- LEI, L. and FITHIAN, W. (2018). AdaPT: an interactive procedure for multiple testing with side information. *Journal of the Royal Statistical Society, Series B* **80** 649–679.
- LI, Q., GLOUDEMANS, M. J., GEISINGER, J. M., FAN, B., AGUET, F., SUN, T., RAMASWAMI, G., LI, Y. I., MA, J.-B., PRITCHARD, J. K. et al. (2022). RNA editing underlies genetic risk of common inflammatory diseases. *Nature* **608** 569–577.

- LIN, W., WALL, J. D., LI, G., NEWMAN, D., YANG, Y., ABNEY, M., VANDEBERG, J. L., OLIVIER, M., GILAD, Y. and COX, L. A. (2024). Genetic regulatory effects in response to a high-cholesterol, high-fat diet in baboons. *Cell Genomics* **4** 100509.
- LIU, C. and RUBIN, D. B. (1998). Maximum likelihood estimation of factor analysis using the ECME algorithm with complete and incomplete data. *Statistica Sinica* **8** 729–747.
- LIU, Y., CARBONETTO, P., TAKAHAMA, M., GRUENBAUM, A., XIE, D., CHEVRIER, N. and STEPHENS, M. (2023). A flexible model for correlated count data, with application to analysis of gene expression differences in multi-condition experiments. *arXiv* **2210.00697**.
- LLAMOSAS, N., ARORA, V., VIJ, R., KILINC, M., BIJOCH, L., ROJAS, C. et al. (2020). SYNGAP1 controls the maturation of dendrites, synaptic function, and network activity in developing human neurons. *Journal of Neuroscience* **40** 7980–7994.
- LUO, L., SHEN, J., ZHANG, H., CHHIBBER, A., MEHROTRA, D. V. and TANG, Z.-Z. (2020). Multi-trait analysis of rare-variant association summary statistics using MTAR. *Nature Communications* **11** 2850.
- MCLACHLAN, G. and PEEL, D. (2000). *Finite mixture models*. John Wiley & Sons, Inc., New York, NY.
- MORRIS, C. N. (1983). Parametric empirical Bayes inference: theory and applications. *Journal of the American Statistical Association* **78** 47–55.
- NATRI, H. M., DEL AZODI, C. B., PETER, L., TAYLOR, C. J., CHUGH, S., KENDLE, R. et al. (2024). Cell-type-specific and disease-associated expression quantitative trait loci in the human lung. *Nature Genetics* **56** 595–604.
- PICKRELL, J. K., BERISA, T., LIU, J. Z., SÉGUREL, L., TUNG, J. Y. and HINDS, D. A. (2016). Detection and interpretation of shared genetic influences on 42 human traits. *Nature Genetics* **48** 709–717.
- ROBBINS, H. (1951). Asymptotically subminimax solutions of compound statistical decision problems. In *Proceedings of the Second Berkeley Symposium on Mathematical Statistics and Probability, 1951, vol. II* 131–149. University of California Press, Berkeley and Los Angeles, CA.
- RUBIN, D. B. and THAYER, D. T. (1982). EM algorithms for ML factor analysis. *Psychometrika* **47** 69–76.
- SHABALIN, A. A. (2012). Matrix eQTL: ultra fast eQTL analysis via large matrix operations. *Bioinformatics* **28** 1353–1358.
- SOLIAI, M. M., KATO, A., HELLING, B. A., STANHOPE, C. T., NORTON, J. E., NAUGHTON, K. A. et al. (2021). Multi-omics colocalization with genome-wide association studies reveals a context-specific genetic mechanism at a childhood onset asthma risk locus. *Genome Medicine* **13** 157.
- SOLLIS, E., MOSAKU, A., ABID, A., BUNIELLO, A., CERZO, M., GIL, L. et al. (2022). The NHGRI-EBI GWAS Catalog: knowledgebase and deposition resource. *Nucleic Acids Research* **51** D977–D985.
- STEPHENS, M. (2017). False discovery rates: a new deal. *Biostatistics* **18** 275–294.
- SUN, L. (2020). Topics on Empirical Bayes Normal Means, PhD thesis, University of Chicago, Chicago, IL.
- TIPPING, M. E. and BISHOP, C. M. (1999). Probabilistic principal component analysis. *Journal of the Royal Statistical Society, Series B* **61** 611–622.
- TURCHIN, M. C. and STEPHENS, M. (2019). Bayesian multivariate reanalysis of large genetic studies identifies many new associations. *PLoS Genetics* **15** e1008431.
- UDLER, M. S., KIM, J., VON GROTHUSS, M., BONÀS-GUARCH, S., COLE, J. B., CHIOU, J., CHRISTOPHER D. ANDERSON ON BEHALF OF METASTROKE AND THE ISGC, BOEHNKE, M. et al. (2018). Type 2 diabetes genetic loci informed by multi-trait associations point to disease mechanisms and subtypes: a soft clustering analysis. *PLoS Medicine* **15** e1002654.
- URBUT, S. M., WANG, G., CARBONETTO, P. and STEPHENS, M. (2019). Flexible statistical methods for estimating and testing effects in genomic studies with multiple conditions. *Nature Genetics* **51** 187–195.
- URBUT, S. M., SELVARAJ, M. S., PAMPANA, A., DATTILO, L., NEALE, B., O'DONNELL, C. J., PELOSO, G. and NATARAJAN, P. (2021). Bayesian multivariate genetic analysis of lipids improves translational insight. *Circulation* **144** A9855–A9855.
- WANG, B. and TITTERINGTON, D. M. (2005). Inadequacy of interval estimates corresponding to variational Bayesian approximations. In *Proceedings of the 10th International Workshop on Artificial Intelligence and Statistics* 373–380.
- WEN, X. and STEPHENS, M. (2014). Bayesian methods for genetic association analysis with heterogeneous subgroups: from meta-analyses to gene-environment interactions. *The Annals of Applied Statistics* **8** 176–203.
- WILLER, C. J., LI, Y. and ABECASIS, G. R. (2010). METAL: fast and efficient meta-analysis of genomewide association scans. *Bioinformatics* **26** 2190–2191.
- WON, J.-H., LIM, J., KIM, S.-J. and RAJARATNAM, B. (2013). Condition-number-regularized covariance estimation. *Journal of the Royal Statistical Society, Series B* **75** 427–450.
- WU, Y., CAO, H., BARANOVA, A., HUANG, H., LI, S., CAI, L. et al. (2020). Multi-trait analysis for genome-wide association study of five psychiatric disorders. *Translational Psychiatry* **10** 209.
- XIE, D. and STEPHENS, M. (2022). Discussion of "Confidence Intervals for Nonparametric Empirical Bayes Analysis". *Journal of the American Statistical Association* **117** 1186–1191.

- YANG, Y., CARBONETTO, P. and STEPHENS, M. (2024a). R package and source code reproducing the analyses for “Improved methods for empirical Bayes multivariate multiple testing and effect size estimation”. <https://doi.org/10.1214/provided-by-typesetter>
- YANG, Y., CARBONETTO, P. and STEPHENS, M. (2024b). Supplementary materials for “Improved methods for empirical Bayes multivariate multiple testing and effect size estimation”. <https://doi.org/10.1214/provided-by-typesetter>
- ZHANG, H., ZHAN, J., JIN, J., ZHANG, J., LU, W., ZHAO, R. et al. (2023). A new method for multiancestry polygenic prediction improves performance across diverse populations. *Nature Genetics* **55** 1757–1768.
- ZHAO, J.-H., PHILIP, L. and JIANG, Q. (2008). ML estimation for factor analysis: EM or non-EM? *Statistics and Computing* **18** 109–123.
- ZHOU, X. and STEPHENS, M. (2014). Efficient multivariate linear mixed model algorithms for genome-wide association studies. *Nature Methods* **11** 407–409.
- ZOU, Y., CARBONETTO, P., XIE, D., WANG, G. and STEPHENS, M. (2024). Fast and flexible joint fine-mapping of multiple traits via the Sum of Single Effects model. *bioRxiv* doi:10.1101/2023.04.14.536893.